Supporting Information

Tuning the Circularly Polarized Phosphorescence of Platinum(II) Complexes through Chiral Cation Strategy

Jiajia Ren,[†a] Tengfei He,[†ad] Haolin Lu,[a] Hebin Wang,[a] Tianyin Shao,[a] Zhaoyu Wang,[a] Yunxin Zhang,[a] Sehrish Gull,[a] Yun Chi,[b] Yu-Wu Zhong,[c] Yongsheng Chen[d] and Guankui Long[*a]

[a.] *Tianjin Key Lab for Rare Earth Materials and Applications, Renewable Energy Conversion and Storage Center (RECAST), Smart Sensing Interdisciplinary Science Center, School of Materials Science and Engineering, Nankai University, Tianjin 300350, China. E-mail: longgk09@nankai.edu.cn.*

[b.] *Department of Materials Science and Engineering, Department of Chemistry, Center of Super-Diamond and Advanced Films (COSDAF), City University of Hong Kong, Hong Kong SAR 999077, China.*

[c.] *CAS Key Laboratory of Photochemistry, Institute of Chemistry, Chinese Academy of Sciences, Beijing 100190, China.*

[d.] *The Centre of Nanoscale Science and Technology and State Key Laboratory of Elemento-Organic Chemistry, Frontiers Science Center for New Organic Matter, College of Chemistry, Nankai University, Tianjin 300071, China.*

† These authors contributed equally to this work.

I Experimental Section

1 Materials

All solution chemicals were commercial available and used as-received without any other refinement unless otherwise specified including *R*-methylbenzylamine (*R*-MBA, ≥99%, Aladdin), *S*-methylbenzylamine (*S*-MBA, ≥99%, Aladdin), potassium tetrachloroplatinate(II) (K_2PtCl_4, 99%, Energy), 2-phenylpyridine (Hppy, 98%, HEOWNS), *R*-3-aminobutanoic acid hydrochloride (*R*-ABA·Cl, 96%, Bide), *S*-3-aminobutanoic acid hydrochloride (*S*-ABA·Cl, 96%, Bide), 1,4-dioxan (99%, GAOFENG), methanol (99%, Aladdin) and trichloromethane (CF, 99.9% , GAOFENG).

2 Experimental methods

2.1 Synthesis of [Pt(ppy)(μ-Cl)]$_2$.

Potassium tetrachloroplatinate (II) (0.85 g, 2.0 mmol) in water (40 ml) was added to a stirred solution of 2-phenylpyridine (0.32 g, 2.1 mmol) in 1,4-dioxan (40 ml).[1] After being stirred at room temperature for three days, the mixture was heated under reflux for three more days. The resulting yellow precipitate was filtered out, and washed successively with 1,4-dioxan, water, methanol, and dichloromethane. The obtained precipitates were dried to get the [Pt(ppy)(μ-Cl)]$_2$ dimer as a yellow microcrystalline solid (0.57 g, 72%). The ^{1}H NMR and ^{13}C NMR spectra of [Pt(ppy)(μ-Cl)]$_2$ are shown in Figures S23 and S24. ^{1}H NMR (400 MHz, DMSO-d_6) δ 9.49 (d, J = 5.7 Hz, 1H), 8.22 (dd, J = 7.6, 1.3 Hz, 1H), 8.19 – 8.09 (m, 2H), 7.78 (dd, J = 7.4, 1.6 Hz, 1H), 7.51 (td, J = 6.3, 2.3 Hz, 1H), 7.16 (ddd, J = 9.2, 7.3, 1.5 Hz, 2H).^{13}C NMR(101 MHz, DMSO-d_6): δ 165.09 (s), 149.31 (s), 144.54 (s), 141.56 (s), 140.31 (s), 133.55 (s), 130.08 (s), 124.94-124.72 (m), 124.33 (s), 122.82 (s), 119.52 (s).

2.2 Synthesis of *R/S*-ABA·[Pt(ppy)Cl$_2$].

A mixture of [Pt(ppy)(μ-Cl)]$_2$ (78.5 mg, 0.1 mmol) and *R/S*-ABACl (27.9 mg, 0.2 mmol) in chloroform (5 mL) was stirred at room temperature for four days.[2] The reaction mixture was filtered and evaporated for getting yellow solid . Yield, 96 mg (0.14 mmol, 92%); The ^{1}H NMR and ^{13}C NMR spectra of *R/S*-ABA·[Pt(ppy)Cl$_2$] are

shown in Figures S25 to S28. ^{1}H NMR (*R*-ABA·[Pt(ppy)Cl$_2$], 400 MHz, DMSO-d_6): δ 12.70 (s, 1H), 9.48 (d, *J* = 6.0 Hz, 1H), 8.15 (td, *J* = 18.4, 15.7, 7.8 Hz, 6H), 7.78 (d, *J* = 7.3 Hz, 1H), 7.51 (s, 1H), 7.16 (p, *J* = 7.3 Hz, 2H), 3.44 (h, *J* = 6.9 Hz, 1H), 2.68 (dd, *J* = 16.7, 5.8 Hz, 1H), 2.56 (m, 1H), 1.22 (d, *J* = 6.5 Hz, 3H). ^{13}C NMR (*R*-ABA·[Pt(ppy)Cl$_2$], 101 MHz, DMSO-d_6): δ 172.00 (s), 165.52 (s), 149.73 (s), 144.98 (s), 142.06 (s), 140.70 (s), 133.97 (s), 130.52 (s), 125.42 (s), 124.80 (s), 123.30 (s), 120.01 (s), 44.10 (s), 38.76 (s), 18.60 (s). ^{1}H NMR (*S*-ABA·[Pt(ppy)Cl$_2$], 400 MHz, DMSO-d_6): δ 12.69 (s, 1H), δ 9.49 (d, *J* = 6.0 Hz, 1H), 8.16 (td, *J* = 18.0, 15.7, 7.8 Hz, 6H), 7.79 (d, *J* = 7.4 Hz, 1H), 7.51 (s, 2H), 7.16 (p, *J* = 7.2 Hz, 3H), 3.44 (h, *J* = 6.7 Hz, 1H), 2.68 (dd, *J* = 16.7, 5.8 Hz, 1H), 2.56 (m, 1H), 1.23 (d, *J* = 6.5 Hz, 3H). ^{13}C NMR (*S*-ABA·[Pt(ppy)Cl$_2$], 101 MHz, DMSO-d_6): δ 172.00 (s), 165.44(s), 149.73(s), 144.98(s), 142.07 (s), 140.70(s), 133.96 (s), 130.52 (s), 125.42 (s), 124.80 (s), 123.30 (s), 120.01 (s), 44.10 (s), 38.77 (s), 18.60 (s). Single crystals were prepared by slowly evaporating *R/S*-ABA·[Pt(ppy)Cl$_2$] in methanol solution at room temperature.

2.3 Synthesis of *R/S*-MBA·Cl.

10 mL *R*/*S*-methylbenzylamine (*R/S*-MBA) was dropped into a 250 mL round bottom flask and then 20 mL HCl was slowly added into it using a constant pressure dropping funnel. Ice bath was employed to control the temperature, the solution was stirred for two days, and then evaporated at 80 °C for 1h to obtain the *R/S*-MBA·Cl precipitates. The obtained precipitates were further washed with diethyl ether and then dried under vacuum to obtain the white solid product. The yield is ≈ 60%, and the ^{1}H NMR and ^{13}C NMR spectra of *R/S*-MBA·Cl are shown in Figures S29 to S32.[3] ^{1}H NMR (*R*-MBA·Cl, 400 MHz, DMSO-d_6): δ 8.77 (s, 3H), 7.55 (d, *J* = 7.4 Hz, 2H), 7.40 (dt, *J* = 22.6, 7.0 Hz, 3H), 4.36 (d, *J* = 6.4 Hz, 1H), 1.53 (d, 6.8 Hz, 3H).^{13}C NMR (*R*-MBA·Cl, 101 MHz, DMSO-d_6): δ=140.00 (s), 129.08 (s), 128.72 (s), 127.36 (s), 50.49 (s), 21.35.^{1}H NMR (*S*-MBA·Cl 400 MHz, DMSO-d_6.): δ=8.79 (s, 3H), 7.55 (d, *J* = 7.4 Hz, 2H), 7.40 (dt, *J* = 22.5, 6.9 Hz, 3H), 4.34 (d, *J* = 5.8 Hz, 1H), 1.53 (d, *J* = 6.6 Hz, 3H). ^{13}C NMR (*R*-MBA·Cl, 101 MHz, DMSO-d_6.): δ=140.00 (s), 129.07 (s), 128.72 (s), 127.37 (s), 50.49 (s), 21.35 (s).

2.4 Synthesis of *R/S*-MBA·[Pt(ppy)Cl$_2$].

A mixture of [Pt(ppy)(μ-Cl)]$_2$ (78.5 mg, 0.1 mmol) and *R/S*-MBACl (31.5 mg, 0.2 mmol) in cholroform (5 mL) was stirred at room temperature for two days. The reaction mixture was filtered and evaporated to get yellow solid. Yield, 108 mg (0.14 mmol, 98%); The ^{1}H NMR and ^{13}C NMR spectra of *R/S*-MBA·[Pt(ppy)Cl$_2$] are shown in Figures S33 to S36.^{1}H NMR (*R*-MBA·[Pt(ppy)Cl$_2$], 400 MHz, DMSO-d_6): δ 9.49 (d, *J* = 5.8 Hz, 1H), 8.45 (s, 3H), 8.30-8.18 (m, 1H), 8.18-8.09 (m, 2H), 7.79 (d, *J* = 7.4 Hz, 1H), 7.51 (d, *J* = 7.5 Hz, 3H), 7.41 (dt, *J* = 16.2, 7.3 Hz, 3H), 7.22-7.08 (m, 2H), 4.39 (s, 1H), 1.51 (d, *J* = 6.7 Hz, 3H). ^{13}C NMR (*R*-MBA·[Pt(ppy)Cl$_2$], 101 MHz, DMSO-d_6): δ 165.52 (s), 149.73 (s), 144.98 (s), 142.05 (s), 140.72 (s), 139.80 (s), 133.97 (s), 130.52 (s), 129.13 (s), 128.81 (s), 127.32 (s), 125.44 (s), 124.80 (s), 123.28 (s), 120.00 (s), 50.34 (s), 21.20 (s). ^{1}H NMR (*S*-MBA·[Pt(ppy)Cl$_2$] 400 MHz, DMSO-d_6): δ 9.49 (d, *J* = 5.3 Hz, 1H), 8.46 (s, 3H), 8.25-8.18 (m, 1H), 8.19-8.07 (m, 2H), 7.79 (d, *J* = 7.2 Hz, 1H), 7.51 (d, *J* = 7.3 Hz, 3H), 7.40 (dt, *J* = 23.6, 7.2 Hz, 3H), 7.24-7.07 (m, 2H), 4.40 (s, 1H), 1.51 (d, *J* = 6.6 Hz, 3H).^{13}C NMR (*S*-MBA·[Pt(ppy)Cl$_2$], 101 MHz, DMSO-d_6): δ 165.53 (s), 149.73 (s), 144.99 (s), 142.06 (s), 140.72 (s), 139.78 (s), 133.98 (s), 130.53 (s), 129.14 (s), 128.83 (s), 127.31 (s), 125.44 (s), 124.80 (s), 123.29 (s), 120.01 (s), 50.31 (s), 21.18 (s). Single crystals were prepared by slowly evaporating *R/S*-MBA·[Pt(ppy)Cl$_2$] in methanol solution at room temperature.

3 Characterization Methods

3.1 X-ray crystallographic analysis.

Single crystal X-ray diffraction (XRD) data were collected on a Rigaku XtalAB PRO MM007 DW diffractometer with a Cu-Kα X-ray source (wavelength = 1.54178 Å) .The structures were solved by direct method using Olex2 software.[4] The structures were drawn from CIFs by using Mercury software. Powder diffraction data were obtained on a powder diffractometer (Rigaku Smart Lab 3kW) equipped with a Cu-Kα X-ray source.

3.2 Nuclear Magnetic Resonance Spectroscopy (NMR).

^{1}H and ^{13}C NMR spectra were obtained by Bruker AV400 Spectrometer at ambient temperature with DMSO-d_6 or $CDCl_3$ as solvent. Solid-state NMR experiment was carried out by the Bruker Avance III WB 400 NMR spectrometer. Spectra were obtained using a cross-polarization magic angle spinning experiment at 25 °C. The relaxation rates R_1 were obtained by fitting the intensity of individual ^{13}C resonances as a function of the inversion recovery time t.[5]

$$M(t) = M_0[1 - e^{(-t/T_1)}] \qquad \text{(Equation S1)}$$

$$R_1 = 1/T_1 \qquad \text{(Equation S2)}$$

where M(t) is the resonance at time t, and M_0 is the resonance intensity at time t=0. The ^{13}C spin-lattice relaxation times in the rotating frame, T_1, is determined by the least-squares fit using the experimental data.

3.3 Thermal gravimetric analysis.

TGA was carried out under a continuous flow of nitrogen gas on a TGA/DSC instrument (METTLER TOLEDO). The samples (~ 20 mg) were heated in aluminum crucibles at a temperature ramp rate of 10 °C min^{-1}.

3.4 Photophysical properties.

UV/visible-diffuse-reflectance spectra were obtained by Cary 5000 UV-visible-NIR spectrophotometer. Steady-state Photoluminescence (PL) and time-resolved photoluminescence (TRPL) were measured by Spectrofluorometer FLS1000 with lamp and pulsed laser, respectively

3.5 CD and CPL spectra.

The measurements of Circular dichroism (CD) spectra were performed under ambient conditions on a JASCO J-1200 CD spectrometer. The samples for CD measurement were prepared though pressing the *R/S*-MBA·[Pt(ppy)Cl_2] and *R/S*-ABA·[Pt(ppy)Cl_2] powder and KBr powder (*R/S*-MBA·[Pt(ppy)Cl_2] or *R/S*-ABA·[Pt(ppy)Cl_2]:KBr=1:50, w:w) into a pellet. Circularly polarized photoluminescence (CPL) measurements were conducted on a JASCO CPL-3000 spectrometer. Spin-coated film was prepared on the REESEEN PvS-mini7 spin-coater. All samples for CPL measurement were excited around 360 nm. In the CPL

measurement, three scans for spin-coated PMMA film were accumulated. The PLQYs were measured using an Edinburg FLS-1000 fluorescence spectrometer with SM4 integrating sphere.

3.6 PMMA films preparation.

Poly(methyl methacrylate) (PMMA, density d_{PMMA}=1.188 g cm^{-3}, 100 mg) was dissolved in DCM (4 mL). 25mg of *R/S*-MBA·[Pt(ppy)Cl_2] and *R/S*-ABA·[Pt(ppy)Cl_2] were then mixed with PMMA solution (0.5 mL) for 30 min by ultra-sonication. For spin coating glass slides were washed with acetone, and then 100 μL of the sample that is PMMA mixture in DCM was spin coated at 2500 rpm for 30 s to get the film.

4 Theoretical calculations

The Vienna Ab-initio Simulation Package (VASP) software is used to accomplish the DFT calculations.[6, 7] The projector augmented wave (PAW)[8] method with the Perdew-Burke-Ernzerhof (PBE) functional revised for solids (PBEsol)[9] is selected and the plane-wave cutoff energy is set to 520.0 eV. Geometric structures are fully relaxed until the energy and total forces are converged to 10^{-5} eV and 0.001 eV/Å, respectively. Γ-centered Monkhorst-Pack mesh k points with k-spacing of 0.04 π $Å^{-1}$ are employed for sampling the Brillouin. DFT-D3 method with Becke-Johnson damping (BJ)[10] is applied for van der Waals correction. For the band structure calculation, 20 points are inserted between each pair of high symmetry k points. The VASPKIT codes[11] are used for post-processing analysis.

Density functional theory (DFT)[12] and unrestricted DFT methods were employed to obtain the equilibrium geometries and the vibration frequencies of ground and the lowest triplet excited states within the Gaussian 16 package.[13] The structural optimizations were carried out with the quantum mechanics/molecular mechanics (QM/MM) method in the ONIOM model[14] which were constructed according to the X-ray crystal structures (the detail packing structure of 3×3×2 supercells shown in Figure S1). In the QM/MM calculation, one innermost molecule was treated as a high-layer by an accurate high-level quantum mechanics method and the surrounding molecules were treated as a low-layer by the efficient universal force field (UFF) with charge

equilibrium method, and the QM part was allowed to move while those in the MM part was frozen. The LANL2DZ[15] basis set was applied for the Pt atom, and the 6-311G(d,p) basis set was applied for the others C/N/H/O/Cl atoms within the PBE0-GD3BJ method.[16, 17] The absorption and circular dichroism spectra as well as the transition electronic/magnetic dipole moment are calculated by the time-dependent DFT method based on the optimized S0 geometry, and the simulated circular dichroism spectra red-shifted about 108 nm to match well with the experimental spectra. The structural reorganization energy between ground and excited states is obtained via MOMAP program.[18]

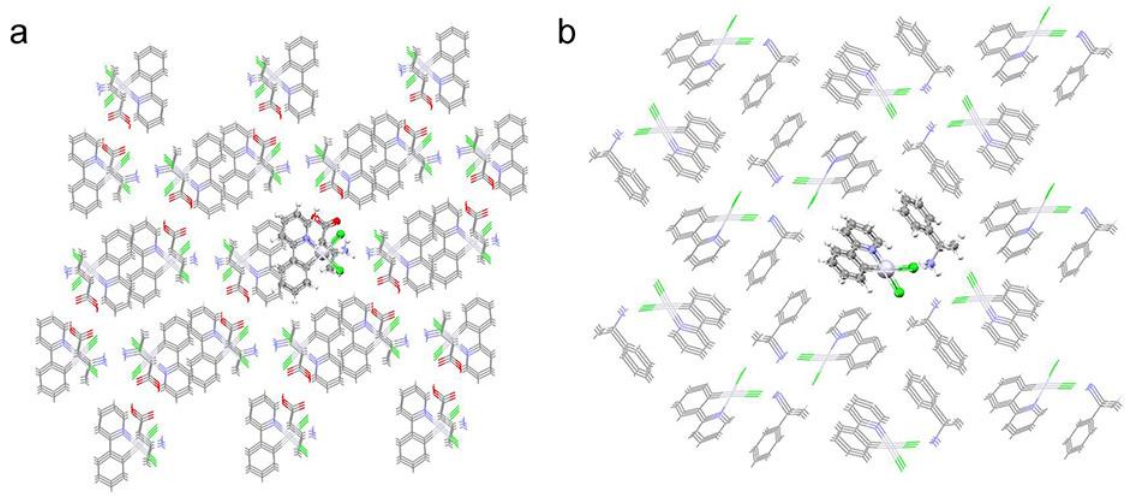

Figure S1. ONIOM model diagrams for (a) *R*-ABA·[Pt(ppy)Cl_2] and (b) *R*-MBA·[Pt(ppy)Cl_2].

II Supplementary Discussion

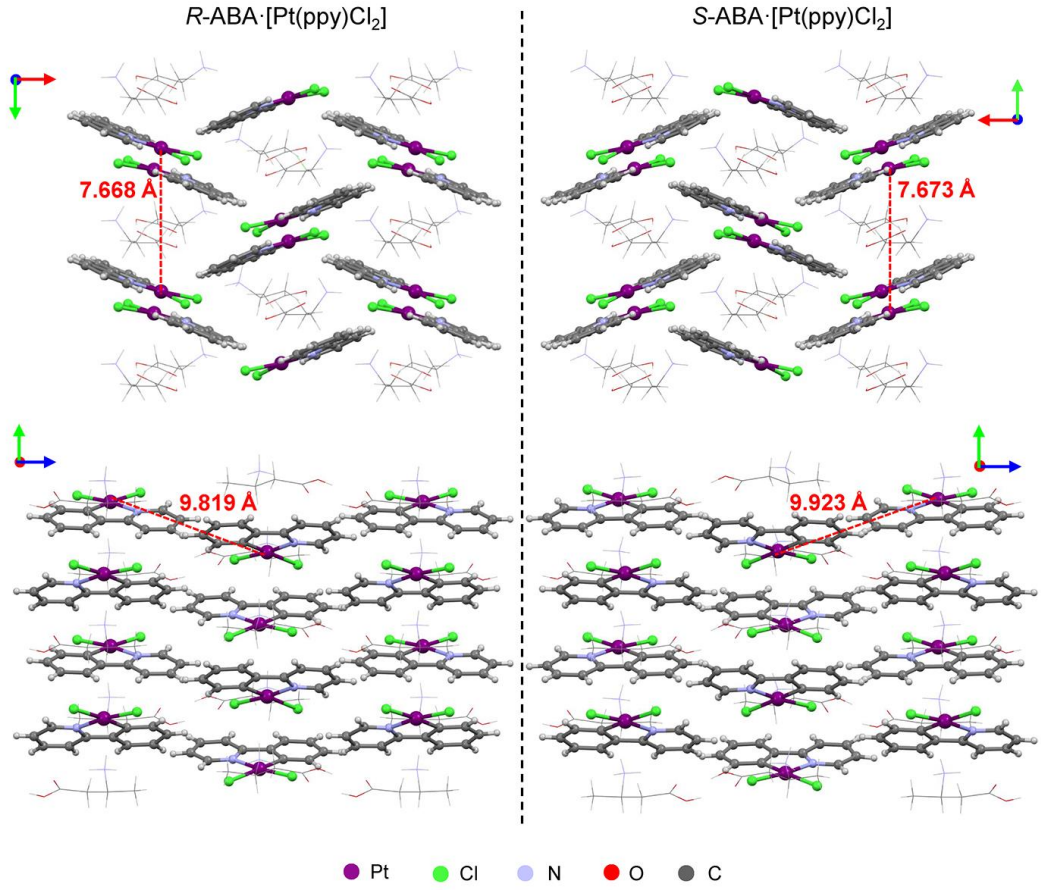

Figure S2. Crystalline structures of *R/S*-ABA·[Pt(ppy)Cl_2].

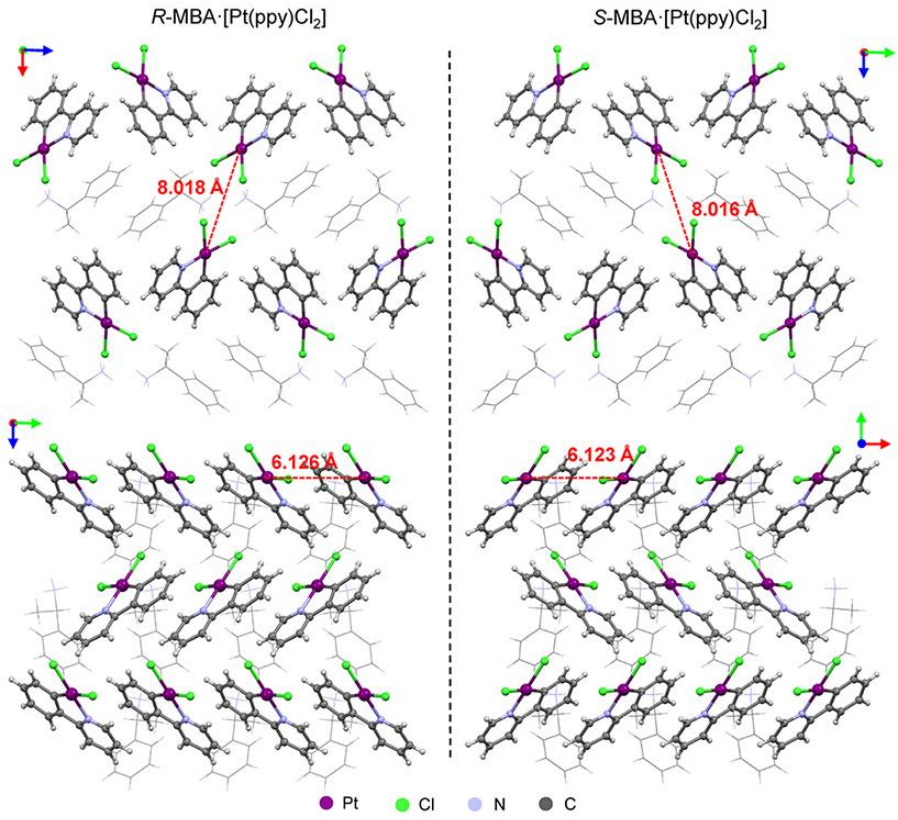

Figure S3. Crystalline structures of *R/S*-MBA·[Pt(ppy)Cl_2].

a

```
ADDSYM Search on ALL NON-H Chemical Types (Max NonFit 20 Perc)
Criteria 1.00 Deg (Metric), 0.25 Ang (Rot), 0.45 Ang (Invl, 0.45 Ang (Transl)
Symm.  Input  Reduced  (Ang)        (Deg) Perc AvrDev.(Ang)          Input Cell
Elem Cell_Raw Cell_Raw   d  Typ Dat Angle Fit  MaxDev.          x     y     z
 n * [ 0 1 0] [ 1 0 0]  7.67  2  1     0   86  0.110  Through    0 0.512     0
                                  C005 -C009 0.248  Glide    1/2     0   1/2
-1 * ================================  100  0.132  at       1/4 0.262   1/4
                                  C11  -C009 0.279

  Reduced-to-Convent       Input-to-Reduced     T = Input-to-Convent:   a' = T a

(     0     1     0 )   (     0    -1     0 )   (     1     0     0 )     Det(T)
(    -1     0     0 ) X (     1     0     0 ) = (     0     1     0 )       =
(     0     0     1 )   (     0     0     1 )   (     0     0     1 )   1.000

Cell Lattice  a       b       c      Alpha   Beta   Gamma  Volume CrystalSystem Laue
Input   mP  13.749   7.668  16.921  90.00  103.63  90.00   1734   monoclinic   2/m
Reduced  P   7.668  13.749  16.921  103.63  90.00  90.00   1734
Convent mP  13.749   7.668  16.921  90.00  103.63  90.00   1734   monoclinic   2/m
:: Origin Shifted to: 0.250, 0.262, 0.250
Missed/Additional Symmetry (Ignore NonFit): Suggested SPGR = P21/n      (No  14)
 *** PLEASE COMPARE with 'CALC ADDSYM EXACT'
```

b

```
ADDSYM Search on ALL NON-H Chemical Types (Max NonFit 20 Perc)
Criteria 1.00 Deg (Metric), 0.25 Ang (Rot), 0.45 Ang (Invl, 0.45 Ang (Transl)
Symm.  Input  Reduced  (Ang)        (Deg) Perc AvrDev.(Ang)          Input Cell
Elem Cell_Raw Cell_Raw   d  Typ Dat Angle Fit  MaxDev.          x     y     z
 n * [ 0 1 0] [ 1 0 0]  7.67  2  1     0  100  0.097  Through    0 0.755     0
                                  C00K -C009 0.188  Glide    1/2     0   1/2
-1 * ================================  100  0.103  at       1/4 0.005   1/4
                                  C00X -C009 0.188

  Reduced-to-Convent       Input-to-Reduced     T = Input-to-Convent:   a' = T a

(     0     1     0 )   (     0    -1     0 )   (     1     0     0 )     Det(T)
(    -1     0     0 ) X (     1     0     0 ) = (     0     1     0 )       =
(     0     0     1 )   (     0     0     1 )   (     0     0     1 )   1.000

Cell Lattice  a       b       c      Alpha   Beta   Gamma  Volume CrystalSystem Laue
Input   mP  13.738   7.673  16.917  90.00  103.62  90.00   1733   monoclinic   2/m
Reduced  P   7.673  13.738  16.917  103.62  90.00  90.00   1733
Convent mP  13.738   7.673  16.917  90.00  103.62  90.00   1733   monoclinic   2/m
:: Origin Shifted to: 0.250, 0.005, 0.250
Missed/Additional Symmetry : Suggested SPGR = P21/n      (No  14)
```

Figure S4. Post-refinement analyses for missing symmetry using PLATON's ADDSYM tool on isolated $[Pt(ppy)Cl_2]^-$ frameworks in (a) *R*-ABA·$[Pt(ppy)Cl_2]$ and (b) *S*-ABA·$[Pt(ppy)Cl_2]$. ABA^+ were manually deleted from the fully refined structure using the Olex2 software. The remaining $[Pt(ppy)Cl_2]^-$ framework is exported into a CIF file for PLATON symmetry analysis. The results indicate a shift from a chiral space group $P2_1$ to an achiral space group.

a

```
ADDSYM Search on ALL NON-H Chemical Types (Max NonFit 20 Perc)
Criteria 1.00 Deg (Metric), 0.25 Ang (Rot), 0.45 Ang (Invl, 0.45 Ang (Transl)
Symm.  Input  Reduced  (Ang)        (Deg) Perc AvrDev.(Ang)          Input Cell
Elem Cell_Raw Cell_Raw   d  Typ Dal Angle Fit  MaxDev.          x      y      z
 2   [ 0 1 0] [ 1 0 0]  6.13  2  1     0  100       0  Through   1/2    0    3/4
  1                                                 0  Screw      0   1/2     0
 2   [ 0 0 1] [ 0-1 0] 13.25  2  1     0  100       0  Through   3/4   1/2     0
  1                                                 0  Screw      0    0    1/2
 2   [ 1 0 0] [ 0 0 1] 23.27  2  1     0  100       0  Through    0    3/4   1/2
  1                                                 0  Screw    1/2    0     0
  Reduced-to-Convent       Input-to-Reduced     T = Input-to-Convent:   a' = T a
(     1     0     0 )   (     0    -1     0 )   (     0    -1     0 )     Det(T)
(     0     1     0 ) X (     0     0     1 ) = (     0     0     1 )       =
(     0     0     1 )   (    -1     0     0 )   (    -1     0     0 )   1.000
Cell Lattice  a       b       c      Alpha   Beta   Gamma  Volume CrystalSystem Laue
Input    oP 23.267   6.126  13.247  90.00  90.00  90.00   1888 orthorhombic   mmm
Reduced   P  6.126  13.247  23.267  90.00  90.00  90.00   1888
Convent  oP  6.126  13.247  23.267  90.00  90.00  90.00   1888 orthorhombic   mmm
:: Origin Shifted to:-0.500, 0.000,-0.500 after Cell Transformation
:: SpaceGroup = P212121      - No Obvious Spacegroup Change Needed/Suggested
```

b

```
ADDSYM Search on ALL NON-H Chemical Types (Max NonFit 20 Perc)
Criteria 1.00 Deg (Metric), 0.25 Ang (Rot), 0.45 Ang (Invl, 0.45 Ang (Transl)
Symm.  Input  Reduced  (Ang)        (Deg) Perc AvrDev.(Ang)          Input Cell
Elem Cell_Raw Cell_Raw   d  Typ Dal Angle Fit  MaxDev.          x      y      z
 2   [ 1 0 0] [ 1 0 0]  6.12  2  1     0  100       0  Through    0    1/4   1/2
  1                                                 0  Screw    1/2     0     0
 2   [ 0 1 0] [ 0-1 0] 13.26  2  1     0  100       0  Through   1/2     0    3/4
  1                                                 0  Screw      0   1/2     0
 2   [ 0 0 1] [ 0 0 1] 23.26  2  1     0  100       0  Through   3/4   1/2     0
  1                                                 0  Screw      0    0    1/2
  Reduced-to-Convent       Input-to-Reduced     T = Input-to-Convent:   a' = T a
(     1     0     0 )   (     1     0     0 )   (     1     0     0 )     Det(T)
(     0    -1     0 ) X (     0    -1     0 ) = (     0     1     0 )       =
(     0     0    -1 )   (     0     0    -1 )   (     0     0     1 )   1.000
Cell Lattice  a       b       c      Alpha   Beta   Gamma  Volume CrystalSystem Laue
Input    oP  6.123  13.255  23.260  90.00  90.00  90.00   1888 orthorhombic   mmm
Reduced   P  6.123  13.255  23.260  90.00  90.00  90.00   1888
Convent  oP  6.123  13.255  23.260  90.00  90.00  90.00   1888 orthorhombic   mmm
:: Origin Shifted to: 0.500, 0.500, 0.500 after Cell Transformation
:: SpaceGroup = P212121      - No Obvious Spacegroup Change Needed/Suggested
```

Figure S5. Post-refinement analyses for missing symmetry using PLATON's ADDSYM tool on isolated $[Pt(ppy)Cl_2]^-$ frameworks in (a) *R*-MBA·$[Pt(ppy)Cl_2]$ and (b) *S*-MBA·$[Pt(ppy)Cl_2]$. MBA^+ was manually deleted from the fully refined structure using the Olex2 software. The remaining $[Pt(ppy)Cl_2]^-$ framework is exported into a CIF file for PLATON symmetry analysis. There is no change from the original $P2_12_12_1$ space group.

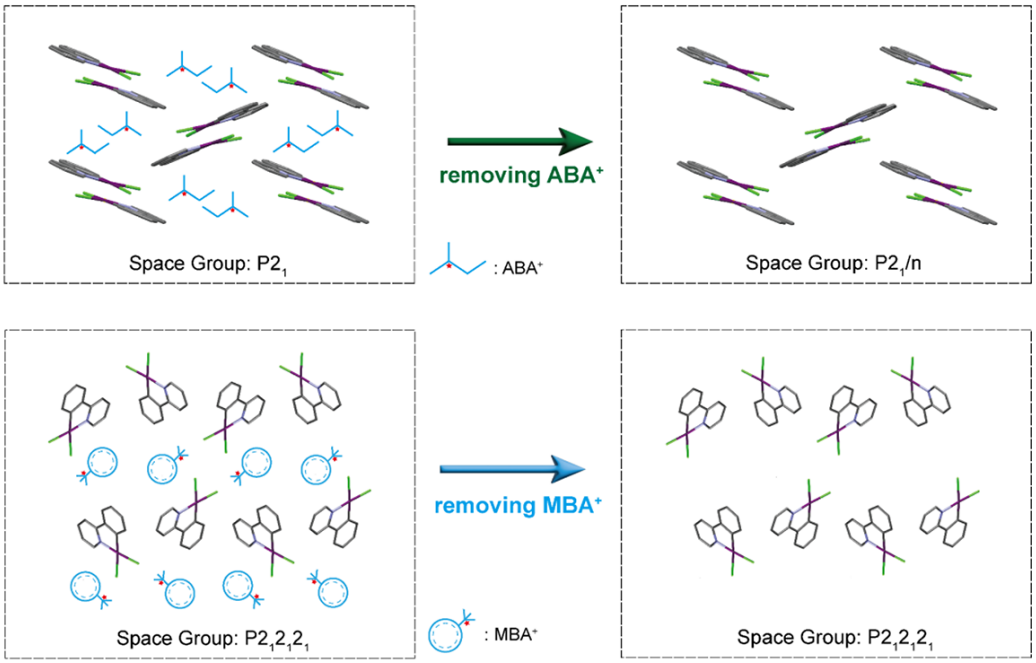

Figure S6. The structure diagrams of *R*-ABA·[Pt(ppy)Cl_2] (top) and *R*-MBA·[Pt(ppy)Cl_2] (bottom) without organic cations.

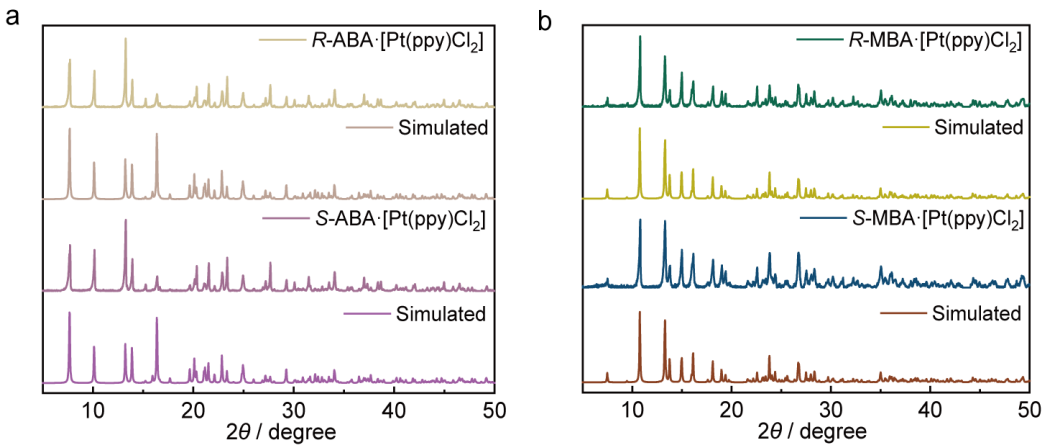

Figure S7. The simulated and experimental powder X-ray diffraction (PXRD) patterns of *R/S*-ABA·[Pt(ppy)Cl_2] and *R/S*-MBA·[Pt(ppy)Cl_2].

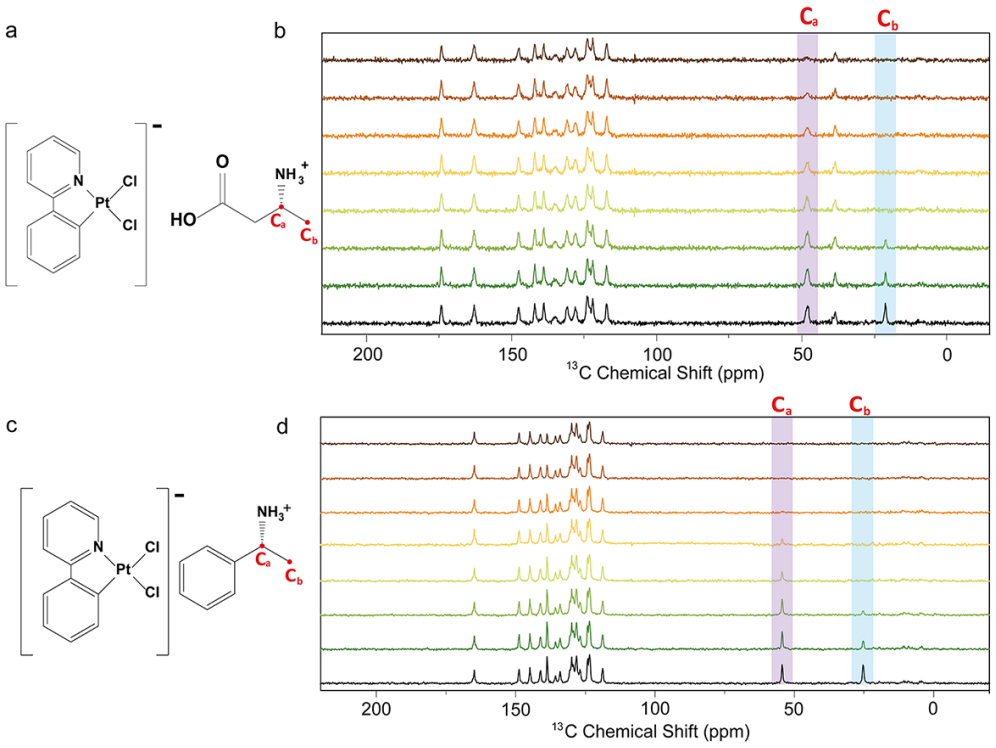

Figure S8. ^{13}C CP-MAS spin-lattice relaxation results of (a, b) *R*-ABA·[Pt(ppy)Cl$_2$] and (c, d) *R*-MBA·[Pt(ppy)Cl$_2$] samples.

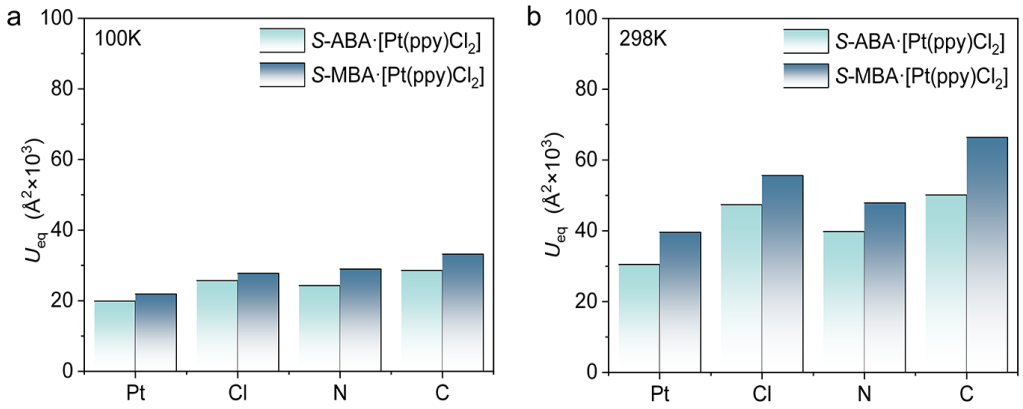

Figure S9. Atomic displacement of Pt, Cl, N and C of *R/S*-ABA·[Pt(ppy)Cl_2] and R/*S*-ABA·[Pt(ppy)Cl_2] at 100 K, respectively.

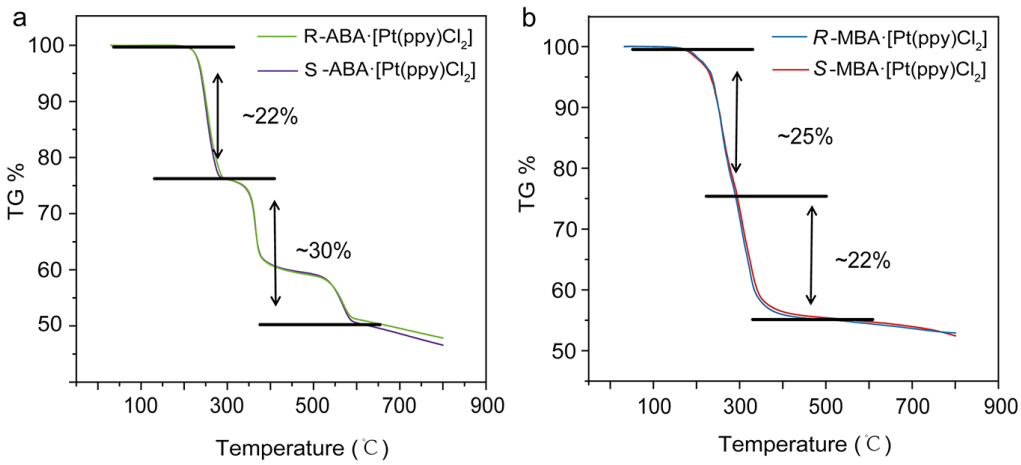

Figure S10. Thermogravimetric analysis curves of (a) *R/S*-ABA·[Pt(ppy)Cl_2] and (b) *R/S*-MBA·[Pt(ppy)Cl_2].

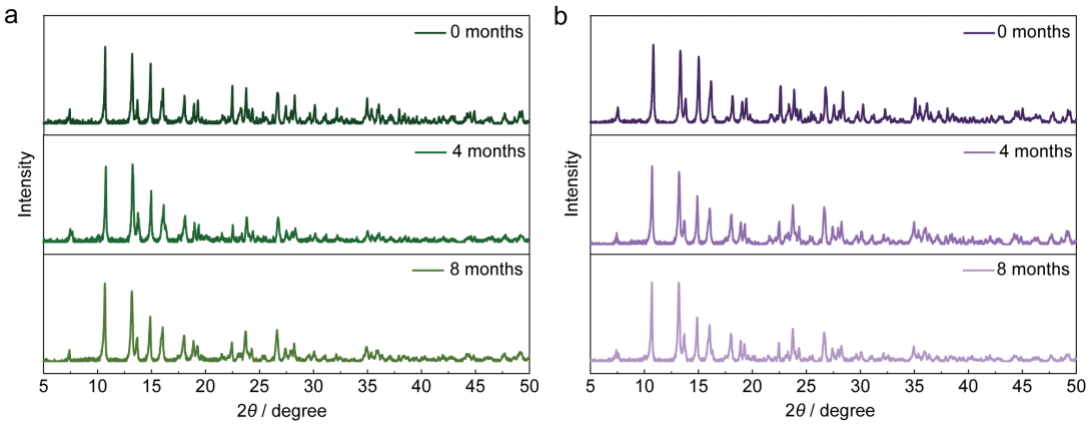

Figure S11. Stability of *R/S*-ABA·[Pt(ppy)Cl_2]. The powder XRD results of (a) *R*-ABA·[Pt(ppy)Cl_2] and (b) *S*-ABA·[Pt(ppy)Cl_2] for as prepared and for the samples kept for 4 and 8 months, respectively.

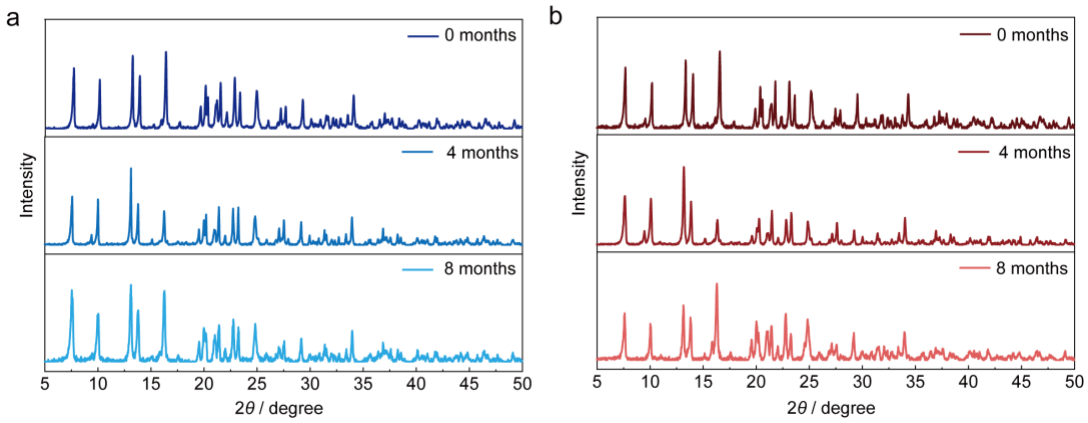

Figure S12. Stability of *R/S*-MBA·[Pt(ppy)Cl_2]. The powder XRD results of (a) *R*-MBA·[Pt(ppy)Cl_2] and (b) *S*-MBA·[Pt(ppy)Cl_2] for as prepared and for the samples kept for 4 and 8 months, respectively.

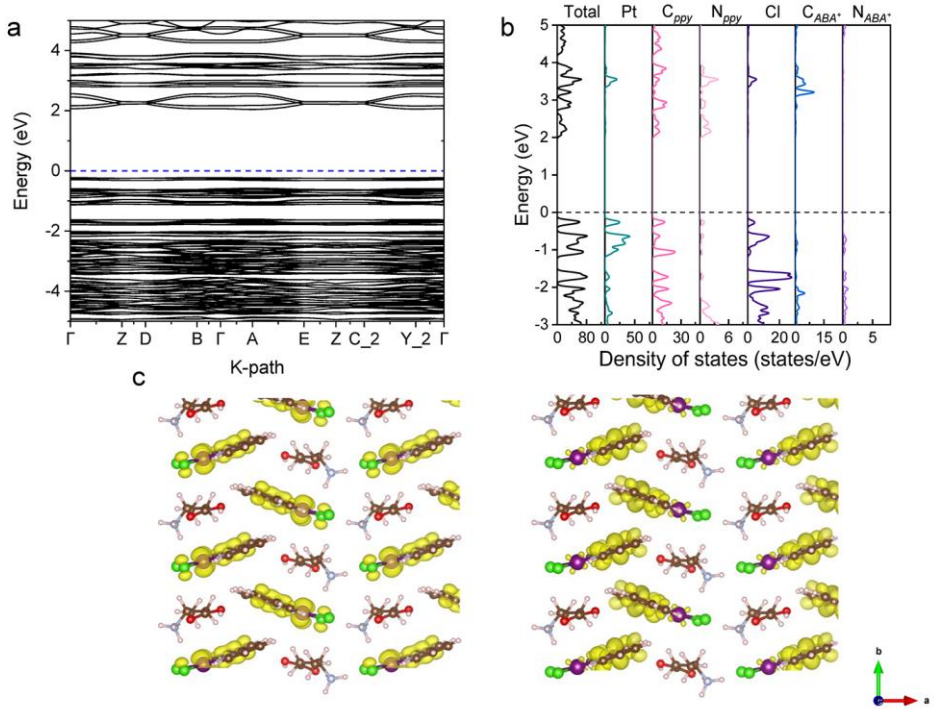

Figure S13. (a) Calculated electronic band structure of *R*-ABA·[Pt(ppy)Cl_2]. (b) Total and partial DOS for *R*-ABA·[Pt(ppy)Cl_2]. (c) Isosurface plots for the wave functions of VBM (below left) and CBM (below right) for *R*-ABA·[Pt(ppy)Cl_2].

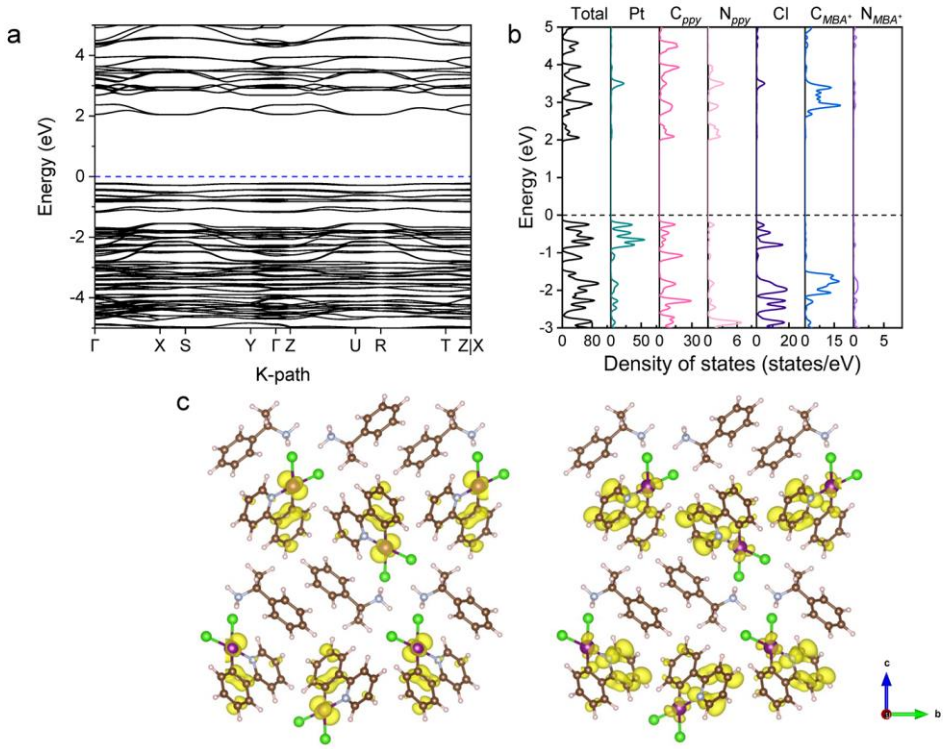

Figure S14. (a) Calculated electronic band structure of *R*-MBA·[Pt(ppy)Cl_2]**.** (b) Total and partial DOS for *R*-MBA·[Pt(ppy)Cl_2]. (c) Isosurface plots for the wave functions of VBM (below left) and CBM (below right) for *R*-MBA·[Pt(ppy)Cl_2].

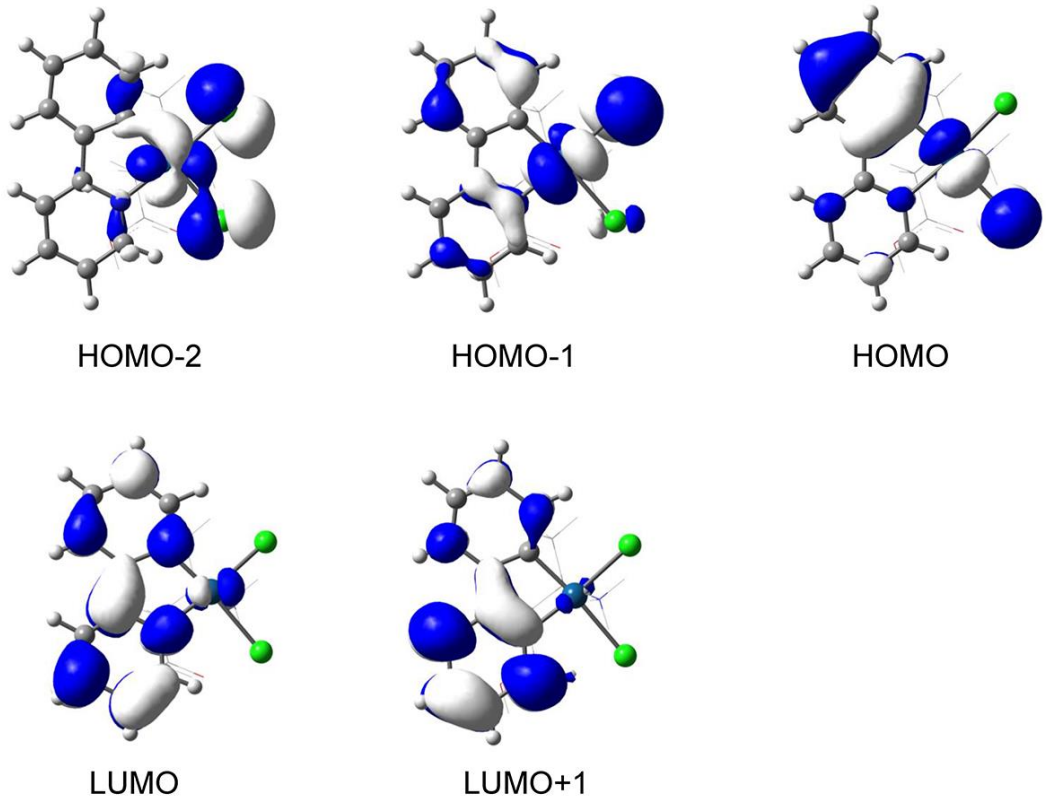

Figure S15. Molecular orbital distributions of *R*-ABA·[Pt(ppy)Cl_2] at ground state.

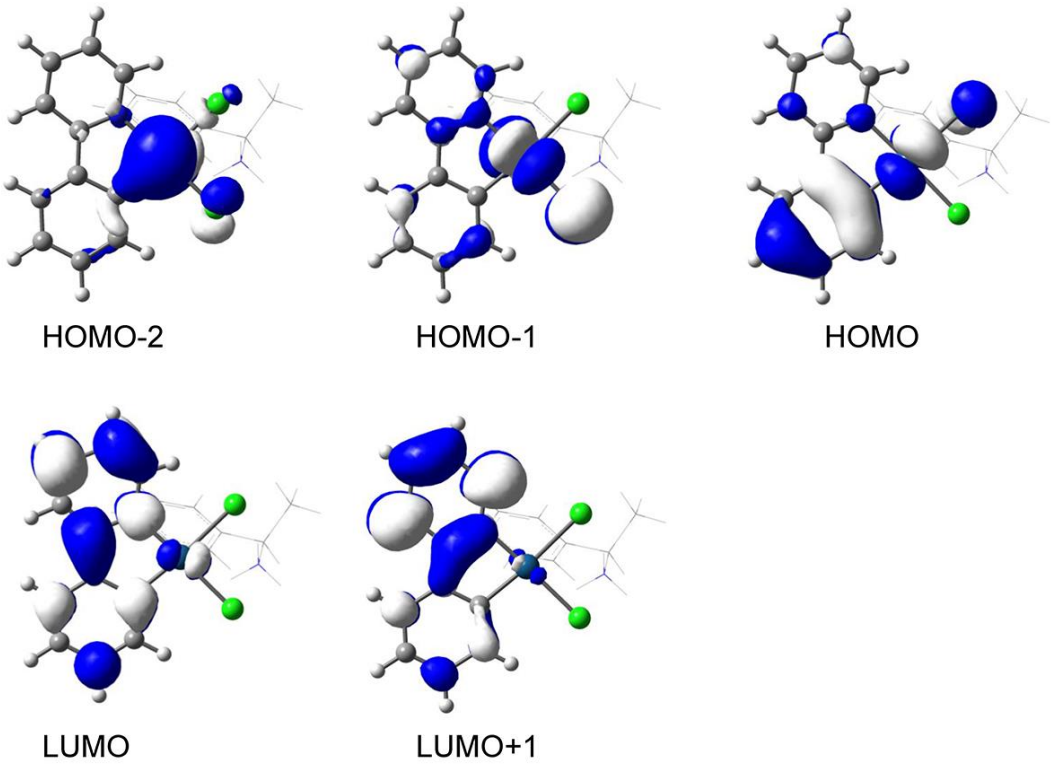

Figure S16. Molecular orbital distributions of *R*-MBA·[Pt(ppy)Cl_2] at ground state.

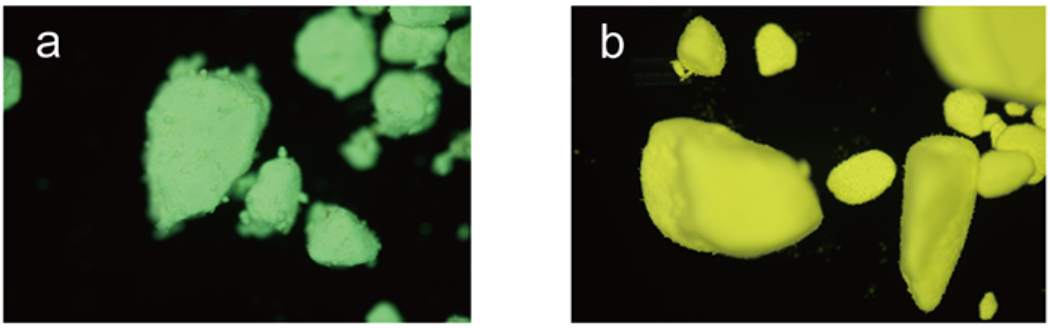

Figure S17. The photographs of (a) *R*-ABA·[Pt(ppy)Cl_2] and (b) *R*-MBA·[Pt(ppy)Cl_2] powders under 365 nm light illumination.

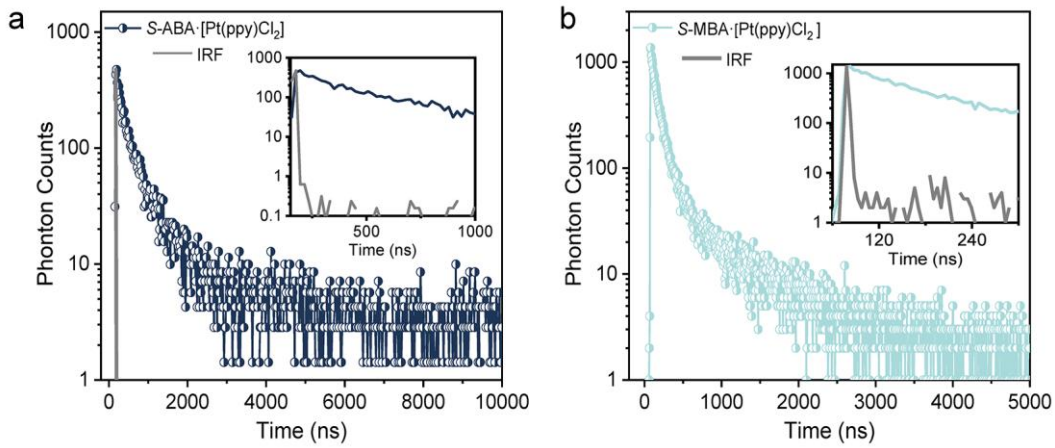

Figure S18. Photoluminescence decay spectra for (a) *S*-ABA·[Pt(ppy)Cl_2] and (b) *S*-MBA·[Pt(ppy)Cl_2] at room temperature.

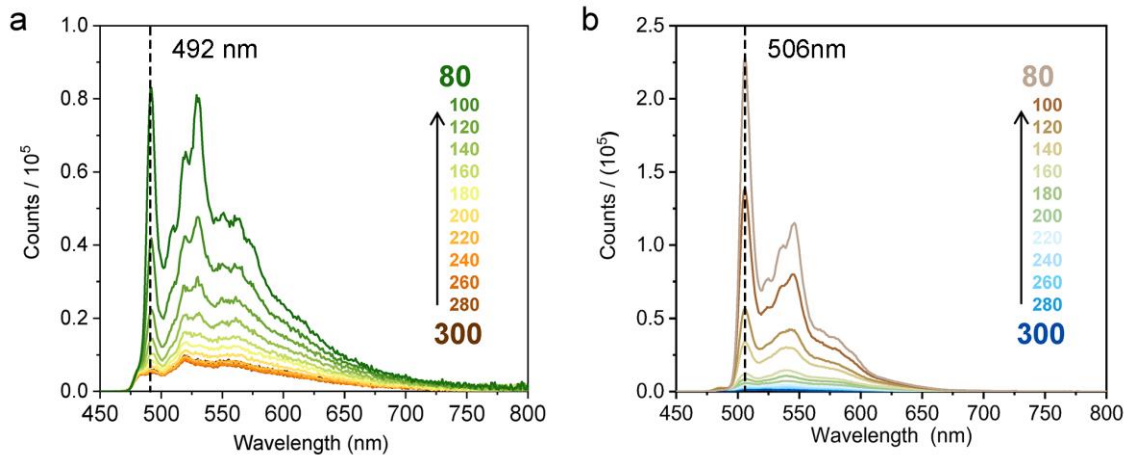

Figure S19. Emission spectra of *R*-ABA·[Pt(ppy)Cl_2] (a) and *R*-MBA·[Pt(ppy)Cl_2] (b) at various temperatures (from 300 K to 80 K).

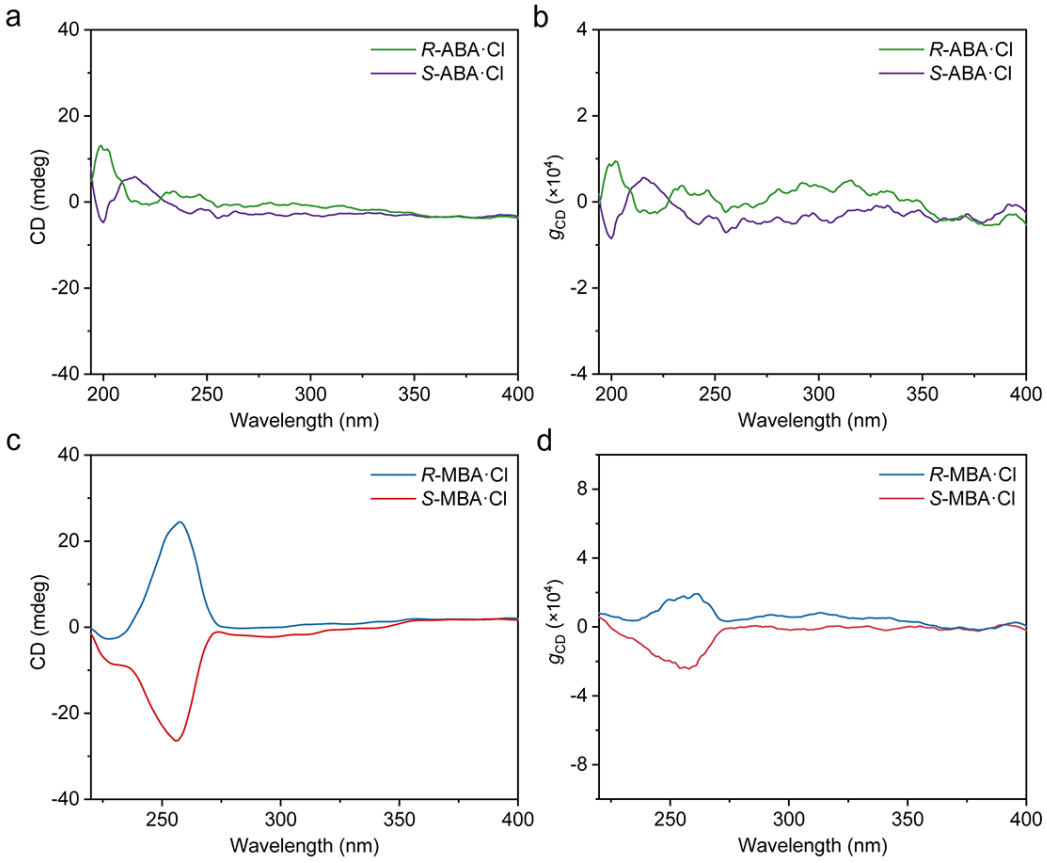

Figure S20. Measured CD spectra and absorption asymmetric factors (g_{abs}) of *R/S*-ABA·Cl and *R/S*-MBA·Cl in cholroform solution.

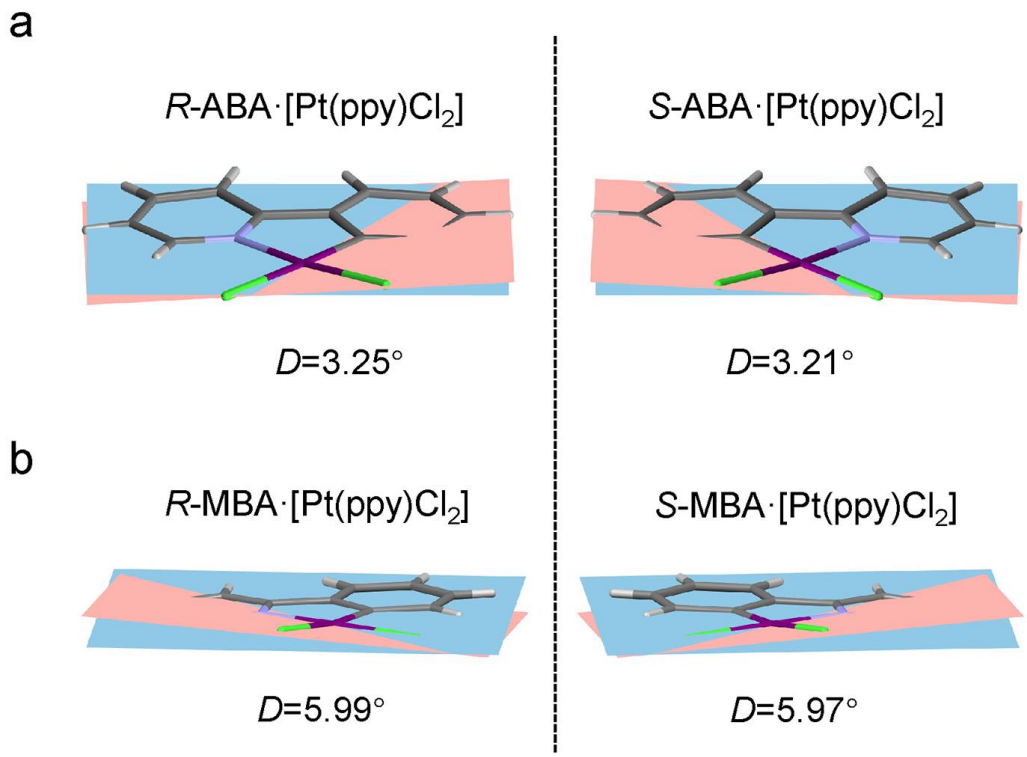

Figure S21. The dihedral angle (D) illustrations of the chiral cation-induced structural deformation of $[Pt(ppy)Cl_2]^-$ for *R/S*-ABA·$[Pt(ppy)Cl_2]$ at single crystals.

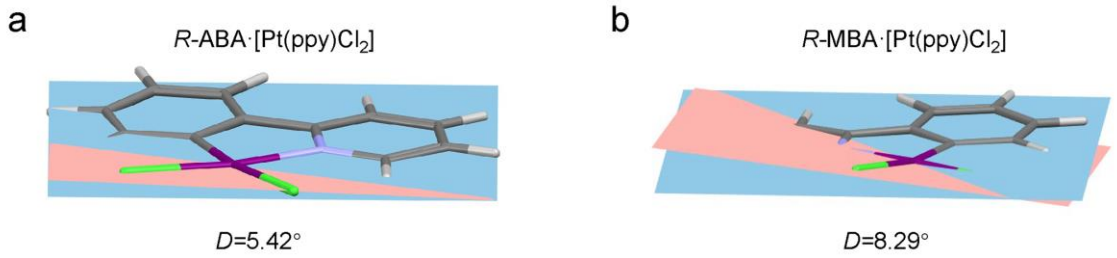

Figure S22. The dihedral angle (D) illustrations of the chiral cation-induced structural deformation of $[Pt(ppy)Cl_2]^-$ for *R*-ABA·$[Pt(ppy)Cl_2]$ at ground state.

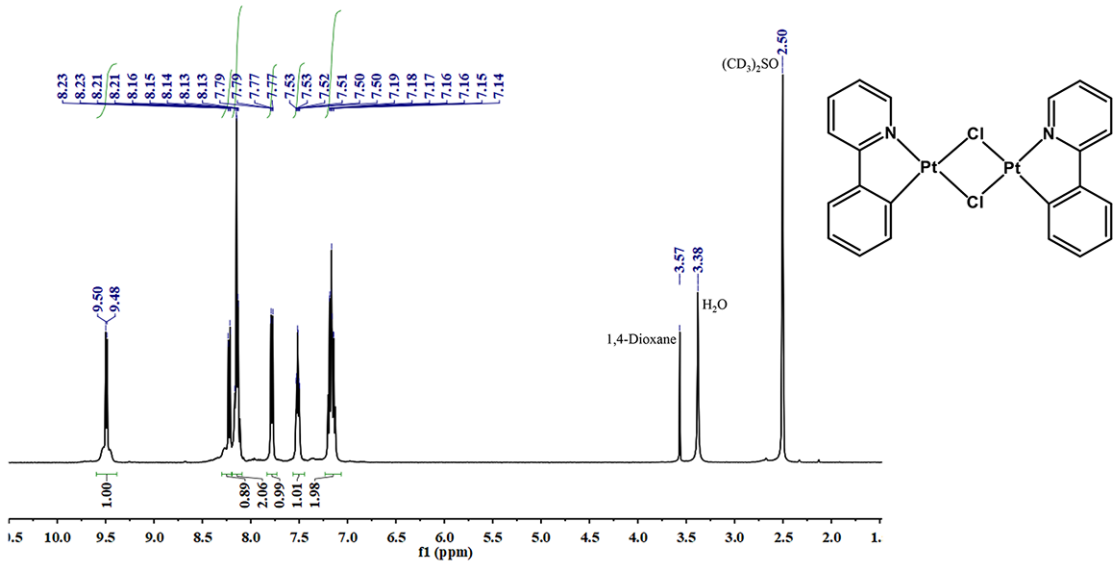

Figure S23. ^{1}H NMR spectra of [Pt(ppy)(μ-Cl)]$_2$ in DMSO-d_6.

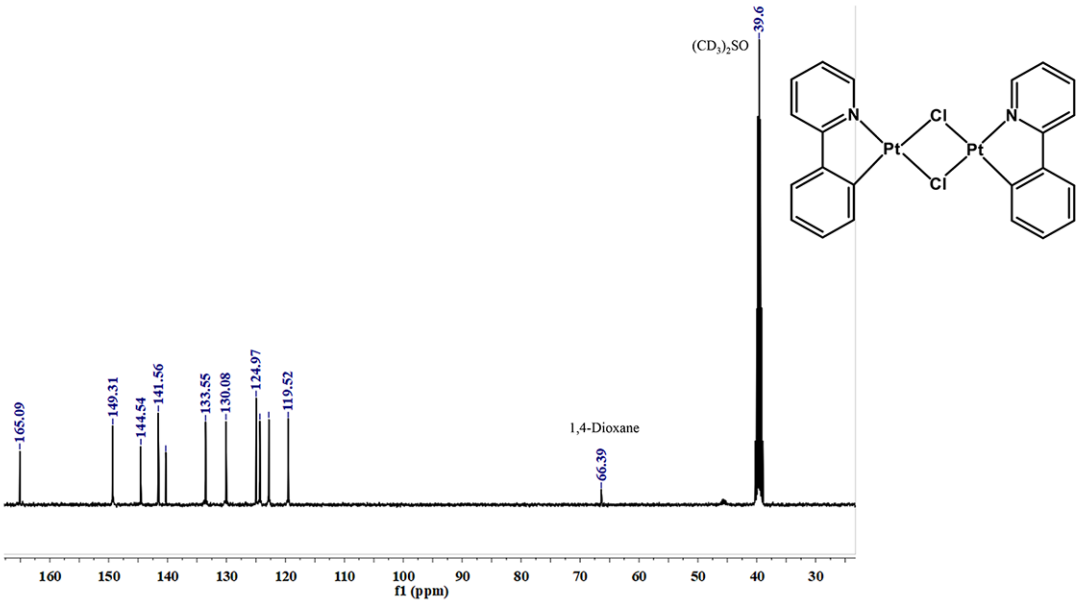

Figure S24. ^{13}C NMR spectra of [Pt(ppy)(μ-Cl)]$_2$ in DMSO-d_6.

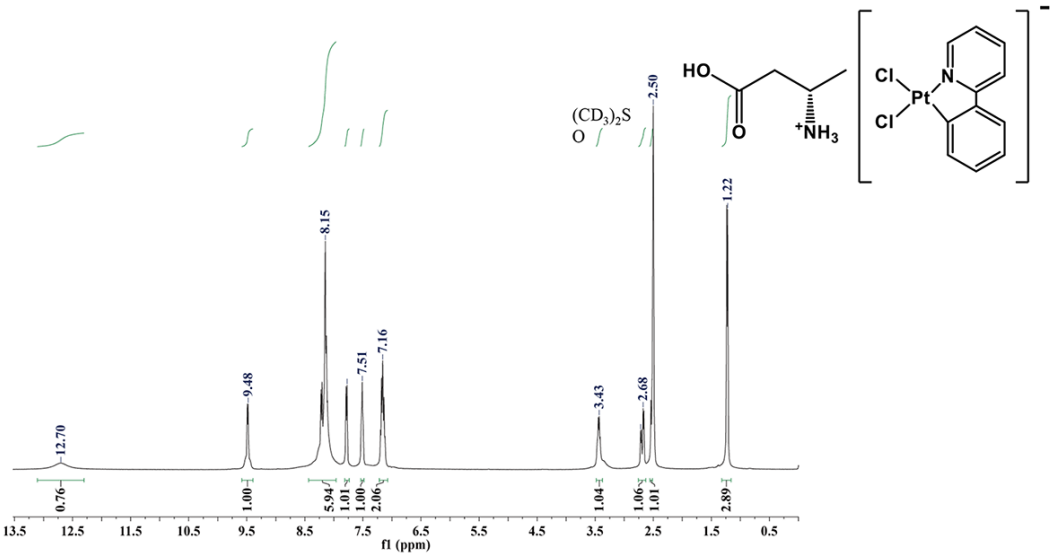

Figure S25. ^{1}H NMR spectra of *R*-ABA·[Pt(ppy)Cl_2] in DMSO-d_6.

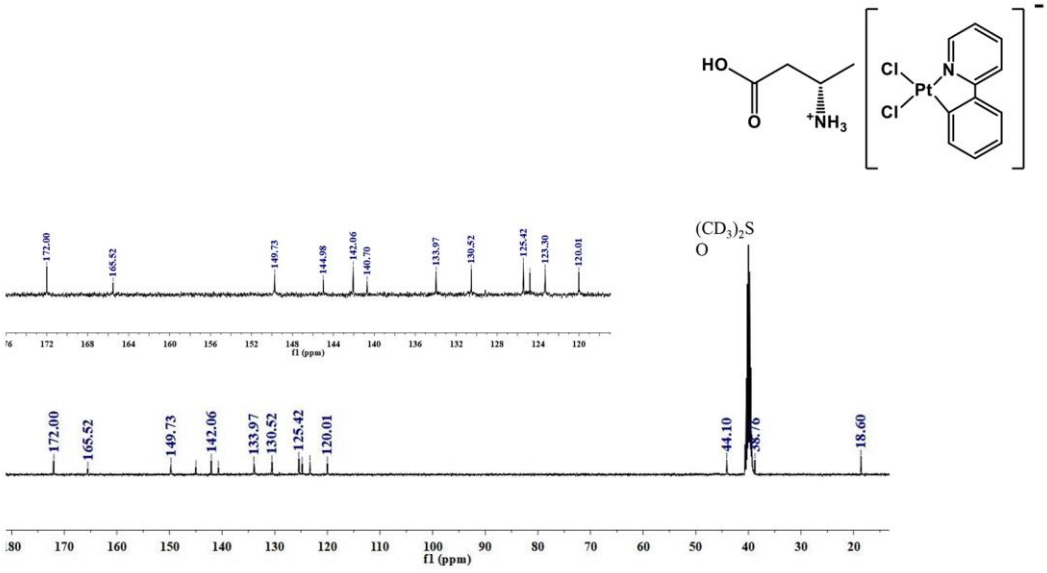

Figure S26. ^{13}C NMR spectra of *R*-ABA·[Pt(ppy)Cl_2] in DMSO-d_6.

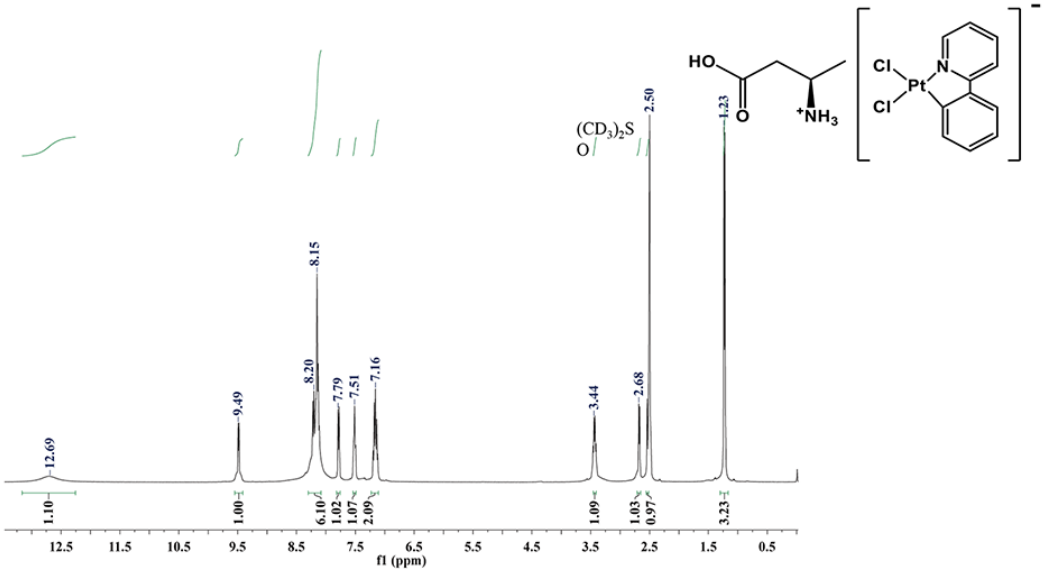

Figure S27. ^{1}H NMR spectra of *S*-ABA·[Pt(ppy)Cl$_2$] in DMSO-d_6.

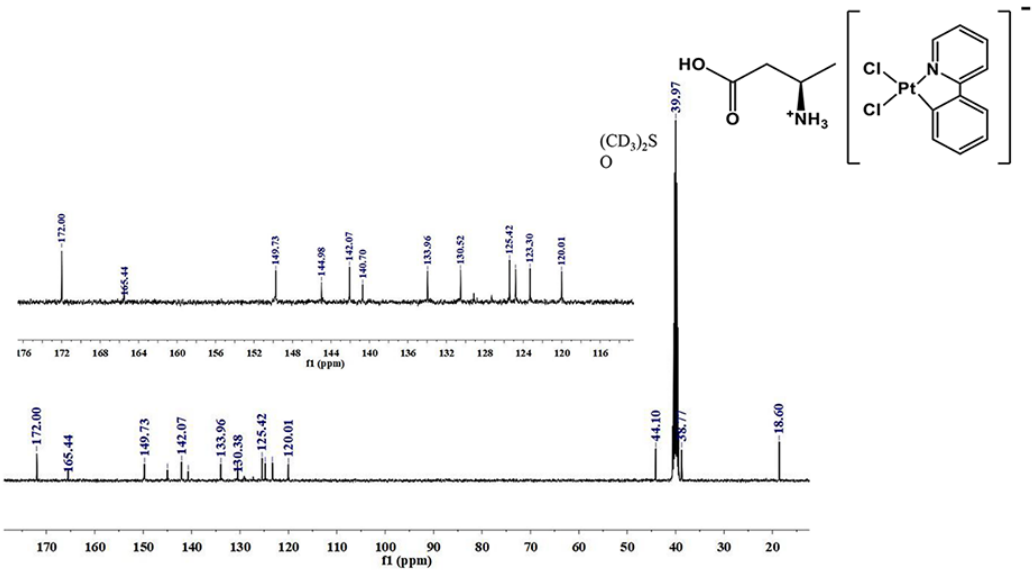

Figure S28. ^{13}C NMR spectra of *S*-ABA·[Pt(ppy)Cl$_2$] in DMSO-d_6.

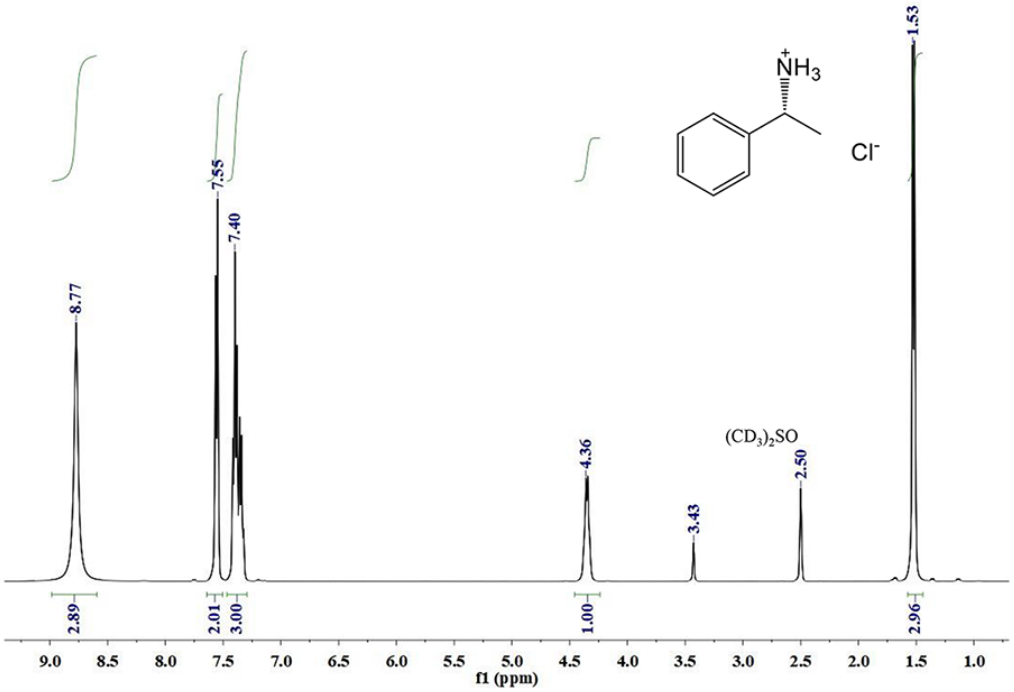

Figure S29. ^{1}H NMR spectra of *R*-MBACl in DMSO-d_6.

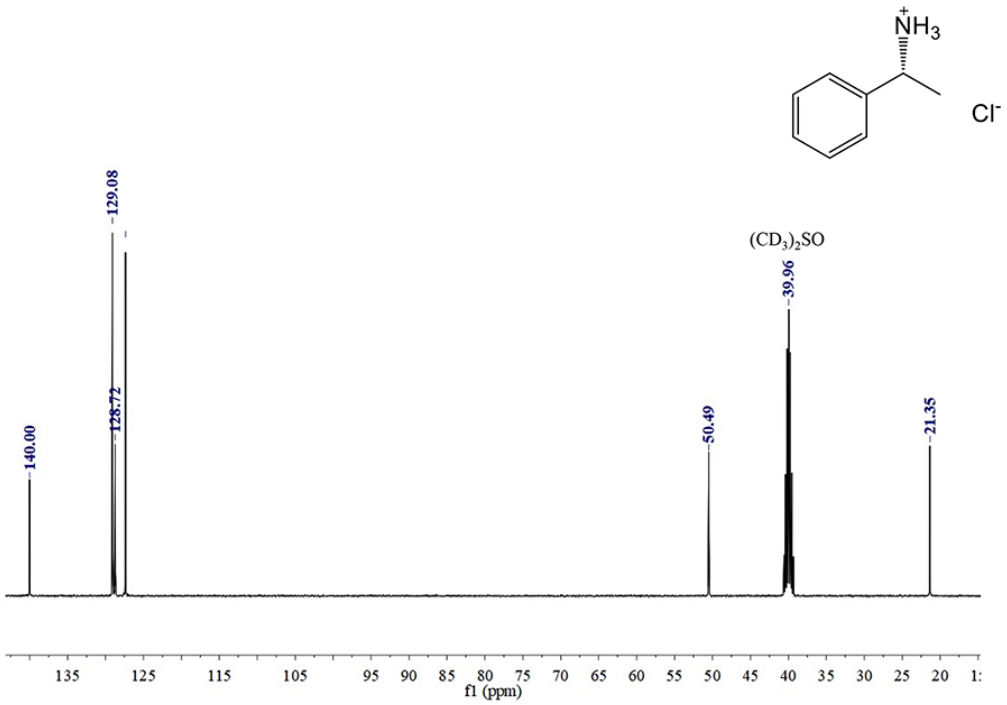

Figure S30. ^{13}C NMR spectra of *R*-MBACl in DMSO-d_6.

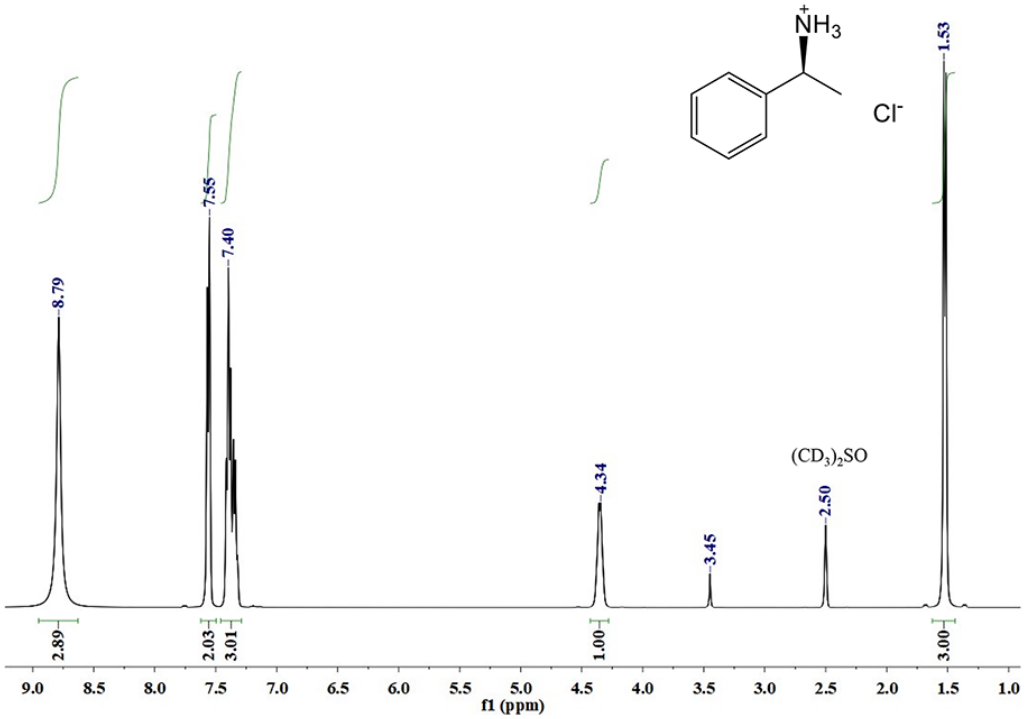

Figure S31. ^{1}H NMR spectra of *S*-MBACl in DMSO-d_6.

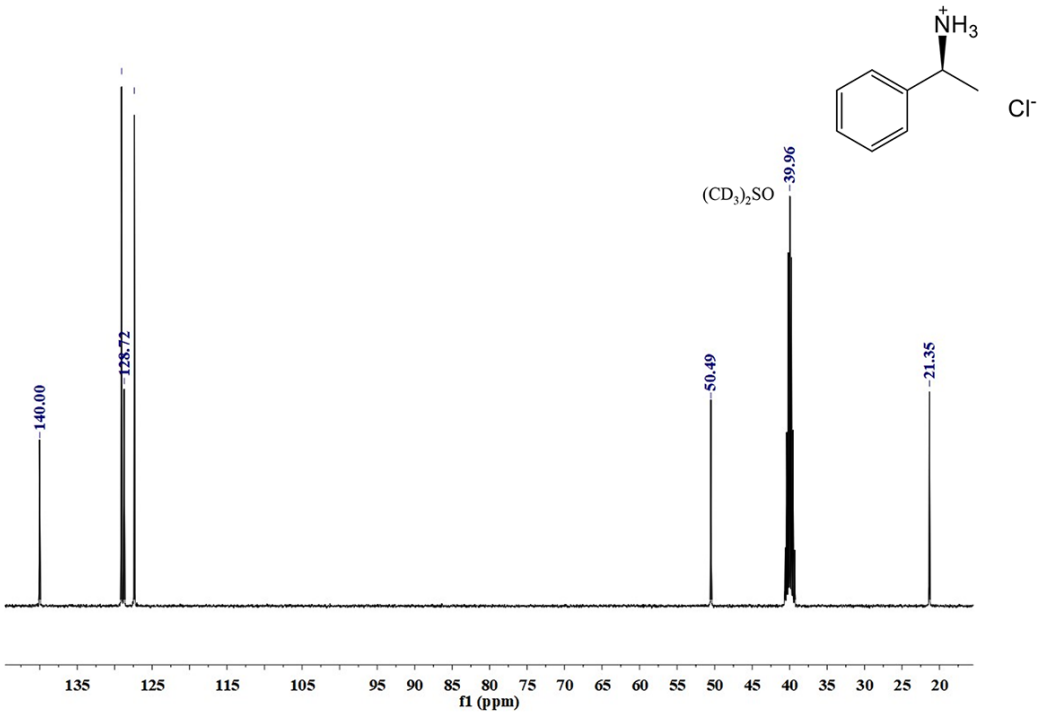

Figure S32. ^{13}C NMR spectra of *S*-MBACl in DMSO-d_6.

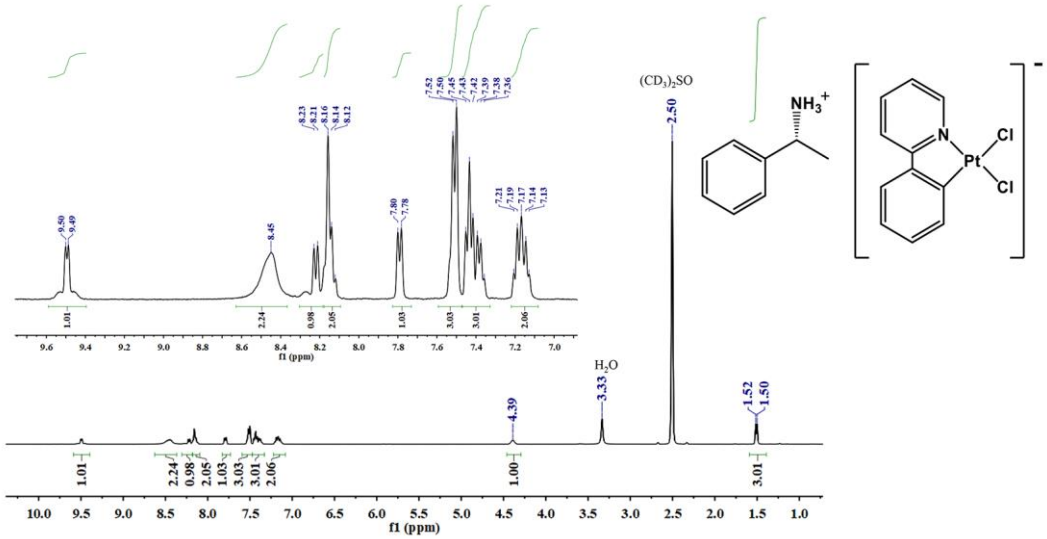

Figure S33. ^{1}H NMR spectra of *R*-MBA·[Pt(ppy)Cl$_2$] in DMSO-d_6.

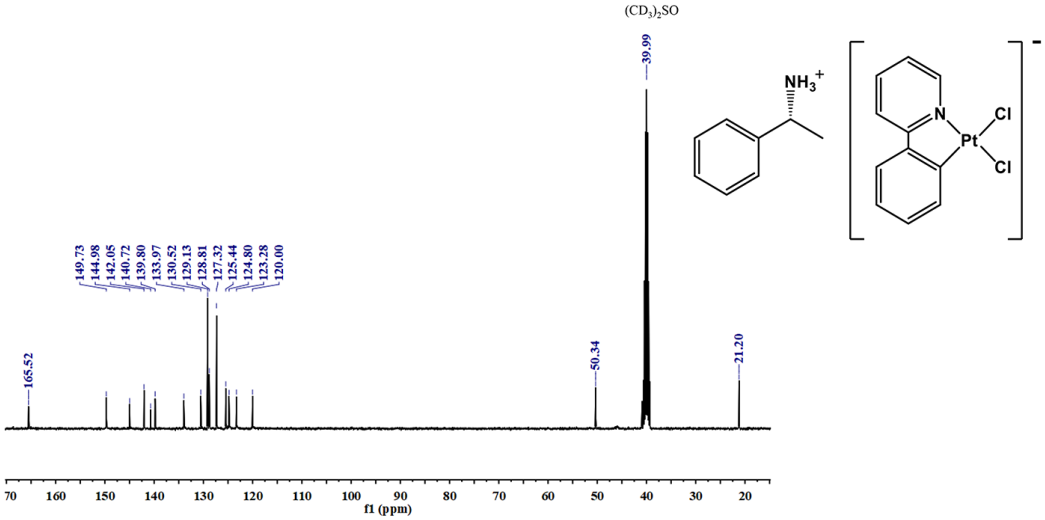

Figure S34. ^{13}C NMR spectra of *R*-MBA·[Pt(ppy)Cl$_2$] in DMSO-*d*$_6$.

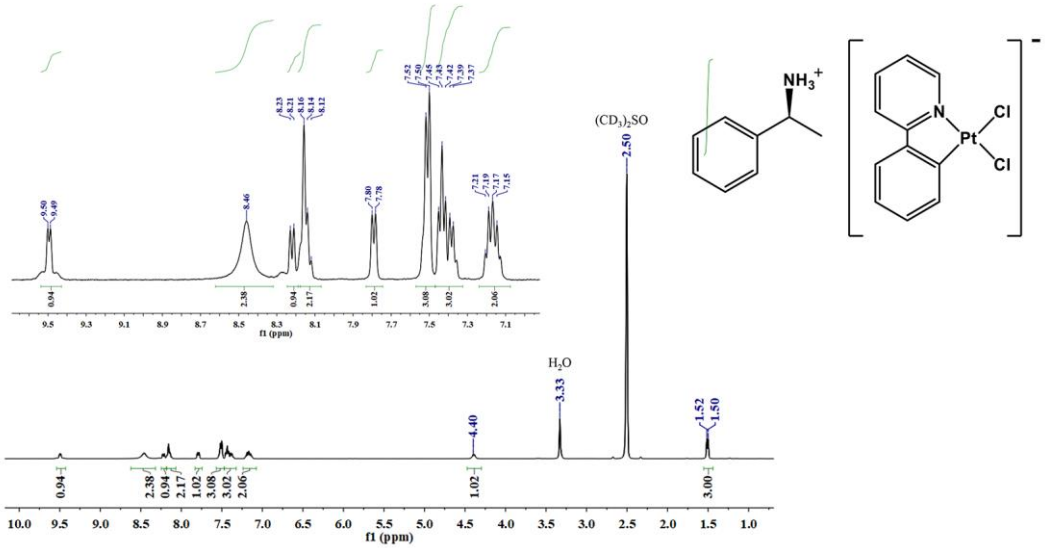

Figure S35. ^{1}H NMR spectra of *S*-MBA·[Pt(ppy)Cl$_2$] in DMSO-d_6.

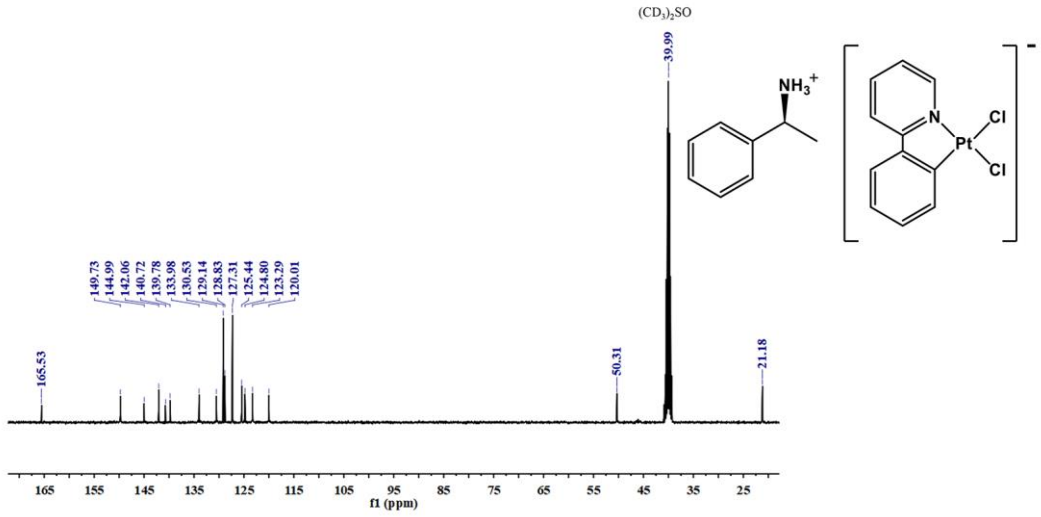

Figure S36. ^{13}C NMR spectra of *S*-MBA·[Pt(ppy)Cl_2] in DMSO-d_6.

Table S1. The crystal density of *R*/*S*-ABA·[Pt(ppy)Cl_2] and *R*/*S*-MBA·[Pt(ppy)Cl_2] obtained from the single crystal XRD.

	Temperature, K	$\rho_{calc,}$ g/cm^3	N_{Pt}, mmol/cm^3
R-ABA·[Pt(ppy)Cl_2]	100	2.058	3.927
R-ABA·[Pt(ppy)Cl_2]	298	2.009	3.833
S-ABA·[Pt(ppy)Cl_2]	100	2.055	3.992
S-ABA·[Pt(ppy)Cl_2]	298	2.009	3.833
R-MBA·[Pt(ppy)Cl_2]	100	1.963	3.621
R-MBA·[Pt(ppy)Cl_2]	298	1.908	3.520
S-MBA·[Pt(ppy)Cl_2]	100	1.959	3.614
S-MBA·[Pt(ppy)Cl_2]	298	1.908	3.520

Table S2. The components and proportions of the absorption transition were simulated for *R*-ABA·[Pt(ppy)Cl_2] and *R*-MBA·[Pt(ppy)Cl_2].

Absorption	Electronic transition	*f*	Configuration	MLCT / %	LLCT / %
R-ABA·[Pt(ppy)Cl_2]	$S_0 \rightarrow S_1$	0.0156	HOMO→LUMO (96%)	39.3	14.8
	$S_0 \rightarrow S_3$	0.0401	HOMO-1→LUMO (52%)	40.1	26.5
			HOMO-2→LUMO (27%)		
			HOMO→LUMO+1 (12%)		
R-MBA·[Pt(ppy)Cl_2]	$S_0 \rightarrow S_1$	0.0095	HOMO→LUMO (95%)	46.6	6.4
	$S_0 \rightarrow S_3$	0.048	HOMO-2→LUMO (21%)	55.1	14.9
			HOMO-1→LUMO (60%)		
			HOMO→LUMO+1 (9%)		

Table S3. Molecular orbital (MO) components of *R*-ABA·[Pt(ppy)Cl_2] and *R*-MBA·[Pt(ppy)Cl_2] ground states.

MO	MO composition			Assignment
	Pt	Cl	ppy	
R-ABA·[Pt(ppy)Cl_2]				
LUMO+1	1.5%	0.3 %	93.8 %	π*(ppy)
LUMO	7.1% (2.8%d_{x2-y2}+1.0%d_{yz})	1.2 %	90.8 %	d(Cu)+π*(ppy)
HOMO	56.2% (4.5%d_{x2-y2}+31.8%d_{z2}+10.6%d_{xy}+2.2%d_{xz}+6.9%d_{yz})	7.9 %	35.2 %	d(Pt)+p(Cl)+π(ppy)
HOMO-1	65.5% (19.3%d_{x2-y2}+2.5%d_{z2}+21.8%d_{xy}+1.4%d_{xz}+18.6%d_{yz})	23.1 %	10.9 %	d(Pt)+p(Cl)+π(ppy)
HOMO-2	79.2% (11.2%d_{x2-y2}+1.9%d_{z2}+18.3%d_{xy}+32.3%d_{xz}+3.2%d_{yz})	6.3 %	13.7 %	d(Pt)+p(Cl)+π(ppy)
R-MBA·[Pt(ppy)Cl_2]				
LUMO+1	1.9%	0.2 %	95.7%	π*(ppy)
LUMO	8.3% (1.6%d_{xy}+2.0%d_{yz})	1.4 %	88.6 %	d(Pt)+π*(ppy)
HOMO	49.2% (7.2%d_{x2-y2}+32.5%d_{z2}+3.0%d_{xy}+4.1%d_{xz}+2.3%d_{yz})	16.8 %	33.8 %	d(Pt)+p(Cl)+π(ppy)
HOMO-1	54.7% (4.0%d_{z2}+8.5%d_{xy}+4.6%d_{xz}+37.1%d_{yz})	28.4 %	16.4 %	d(Pt)+p(Cl)+π(ppy)
HOMO-2	46.4% (35.6%d_{x2-y2}+1.7%d_{z2}+6.7%d_{xy}+1.6%d_{xz})	40.2 %	13.1 %	d(Pt)+p(Cl)+π(ppy)

Table S4. Single crystal XRD analysis data and structural refinement for *R*-ABA·[Pt(ppy)Cl_2] at different temperatures.

Temperature/K	100	298
CCDC	2365460	2365461
Crystal system	monoclinic	monoclinic
Space group	$P2_1$	$P2_1$
a/Å	13.74620(10)	13.74920(10)
b/Å	7.54290(10)	7.66790(10)
c/Å	16.79970(10)	16.92060(10)
α/°	90	90
β/°	103.6710(10)	103.6330(10)
γ/°	90	90
Volume/Å^3	1692.55(3)	1733.64(3)
Z	4	4
ρ_{calc} g/cm^3	2.058	2.009
F(000)	1000.0	1000.0
Radiation	Cu Kα (λ = 1.54184)	Cu Kα (λ = 1.54184)
Reflections collected	10528	23651
Independent reflections	4959 [R_{int} = 0.0366, R_{sigma} = 0.0448]	6667 [R_{int} = 0.0624, R_{sigma} = 0.0450]
Data/restraints/parameters	4959/13/402	6667/1/404
Goodness-of-fit on F^2	0.752	0.869
Final *R* indexes [*I*>=2σ (*I*)]	R_1 = 0.0314, wR_2 = 0.0911	R_1 = 0.0390, wR_2 = 0.1089
Final *R* indexes [all data]	R_1 = 0.0338, wR_2 = 0.0947	R_1 = 0.0429, wR_2 = 0.1125
Largest diff. peak/hole / e Å^{-3}	1.42/-1.72	1.79/-2.22
Flack parameter	0.009(15)	0.05(2)

Table S5. Single crystal XRD analysis data and structural refinement for *S*-ABA·[Pt(ppy)Cl_2] at different temperatures.

Temperature/K	100	298
CCDC	2365462	2365463
Crystal system	monoclinic	monoclinic
Space group	$P2_1$	$P2_1$
a/Å	13.7103(4)	13.73760(10)
b/Å	7.5618(3)	7.67280(10)
c/Å	16.8169(6)	16.9169(2)
α/°	90	90
β/°	103.556(3)	103.6160(10)
γ/°	90	90
Volume/Å^3	1694.91(11)	1733.03(3)
Z	4	4
ρ_{calc} g/cm^3	2.055	2.009
F(000)	1000.0	1000.0
Radiation	Cu Kα (λ = 1.54184)	Cu Kα (λ = 1.54184)
Reflections collected	14386	17437
Independent reflections	5933 [R_{int} = 0.0645, R_{sigma} = 0.0706]	6892 [R_{int} = 0.0392, R_{sigma} = 0.0443]
Data/restraints/parameters	5933/13/402	6892/1/402
Goodness-of-fit on F^2	0.991	1.110
Final *R* indexes [*I*>=2σ (*I*)]	R_1 = 0.0406, wR_2 = 0.1017	R_1 = 0.0280, wR_2 = 0.0761
Final *R* indexes [all data]	R_1 = 0.0461, wR_2 = 0.1050	R_1 = 0.0312, wR_2 = 0.0783
Largest diff. peak/hole / e Å^{-3}	2.18/-2.00	0.85/-1.04
Flack parameter	-0.02(2)	0.005(17)

Table S6. Single crystal XRD analysis data and structural refinement for *R*-MBA·[Pt(ppy)Cl_2] at different temperatures

Temperature/K	100	298
CCDC	2365464	2365465
Crystal system	orthorhombic	orthorhombic
Space group	$P2_12_12_1$	$P2_12_12_1$
a/Å	23.2773(4)	23.2671(10)
b/Å	6.02850(10)	6.1257(3)
c/Å	13.0805(2)	13.2471(6)
α/°	90	90
β/°	90	90
γ/°	90	90
Volume/Å^3	1835.55(5)	1888.07(15)
Z	4	4
ρ_{calc} g/cm^3	1.963	1.908
F(000)	1040.0	1040.0
Radiation	Cu Kα (λ = 1.54184)	Mo Kα (λ = 0.71073)
Reflections collected	7961	12683
Independent reflections	3196 [R_{int} = 0.0442, R_{sigma} = 0.0505]	4748 [R_{int} = 0.0313, R_{sigma} = 0.0396]
Data/restraints/parameters	3196/0/219	4748/0/219
Goodness-of-fit on F^2	1.067	0.998
Final *R* indexes [I>=2σ (I)]	R_1 = 0.0387, wR_2 = 0.1055	R_1 = 0.0285, wR_2 = 0.0510
Final *R* indexes [all data]	R_1 = 0.0405, wR_2 = 0.1068	R_1 = 0.0383, wR_2 = 0.0525
Largest diff. peak/hole / e Å^{-3}	2.09/-2.26	0.92/-0.57
Flack parameter	-0.012(15)	-0.005(5)

Table S7. Single crystal XRD analysis data and structure refinement for *S*-MBA·[Pt(ppy)Cl_2] at different temperatures.

Temperature/K	100	298
CCDC	2365466	2365467
Crystal system	orthorhombic	orthorhombic
Space group	$P2_12_12_1$	$P2_12_12_1$
a/Å	6.02970(10)	6.1233(7)
b/Å	13.0932(3)	13.2555(14)
c/Å	23.2882(5)	23.260(3)
α/°	90	90
β/°	90	90
γ/°	90	90
Volume/Å^3	1838.56(7)	1888.0 (4)
Z	4	4
ρ_{calc} g/cm^3	1.959	1.908
F(000)	1040.0	1040.0
Radiation	Cu Kα (λ = 1.54184)	Mo Kα (λ = 0.71073)
Reflections collected	8483	9545
Independent reflections	3185 [R_{int} = 0.1172, R_{sigma} = 0.1166]	3311 [R_{int} = 0.0814, R_{sigma} = 0.0903]
Data/restraints/parameters	3185/30/183	3311/1/183
Goodness-of-fit on F^2	1.021	0.981
Final *R* indexes [I>=2σ (I)]	R_1 = 0.0756, wR_2 = 0.1608	R_1 = 0.0455, wR_2 = 0.0827
Final *R* indexes [all data]	R_1 = 0.0969, wR_2 = 0.1689	R_1 = 0.0726, wR_2 = 0.0888
Largest diff. peak/hole / e Å^{-3}	3.46/-1.86	0.83/-0.59
Flack parameter	-0.05(3)	-0.000(17)

Table S8. Summary of the g_{lum}, electric transition dipole moment ($|\boldsymbol{\mu}_e|$) and magnetic transition dipole moment ($|\boldsymbol{\mu}_m|$) of the CPPL of *R*/*S*-ABA·[Pt(ppy)Cl_2] and *R*/*S*-MBA·[Pt(ppy)Cl_2].

	g_{lum}	$\|\boldsymbol{\mu}_e\|$ [Debye]	$\|\boldsymbol{\mu}_m\|$ [Bohr Mag.]
R-ABA·[Pt(ppy)Cl_2]	$+1.4\times10^{-3}$	1.79	0.06
S-ABA·[Pt(ppy)Cl_2]	-1.8×10^{-3}	1.76	0.09
R-MBA·[Pt(ppy)Cl_2]	$+4.4\times10^{-3}$	2.14	0.26
S-MBA·[Pt(ppy)Cl_2]	-2.8×10^{-3}	1.99	0.15

III Supplementary References

1 D. S. Black, G. B. Deacon and G. L. J. A. J. o. C. Edwards, *Aust. J. Chem.*,1994, **47**, 217-227.

2 M. Yoshida, V. Sääsk, D. Saito, N. Yoshimura, J. Takayama, S. Hiura, A. Murayama, K. Põhako-Esko, A. Kobayashi and M. Kato, *Adv. Opt. Mater.*, 2022, **10**, 2102614.

3 H. Lu, T. He, H. Wu, F. Qi, H. Wang, B. Sun, T. Shao, T. Qiao, H.-L. Zhang, D. Sun, Y. Chen, Z. Tang and G. Long, *Adv. Funct. Mater.*, 2024, **34**, 2308862.

4 K. Momma and F. Izumi, *J. Appl. Crystallogr.*, 2008, **41**, 653-658.

5 A. R. Lim, G. T. Schueneman and B. M. Novak, *Solid State Commun.*, 1999, **109**, 465-470.

6 R. Inoue, R. Kondo and Y. Morisaki, *Chem. Commun.*, 2020, **56**, 15438-15441.

7 G. Kresse and J. Furthmüller, *Phys. Rev. B*, 1996, **54**, 11169-11186.

8 P. E. Blöchl, *Phy. Rev. B*, 1994, **50**, 17953-17979.

9 J. P. Perdew, A. Ruzsinszky, G. I. Csonka, O. A. Vydrov, G. E. Scuseria, L. A. Constantin, X. Zhou and K. Burke, *Phys. Rev. Lett.*, 2008, **100**, 136406.

10 S. Grimme, S. Ehrlich and L. Goerigk, *J. Comput. Chem.*, 2011, **32**, 1456-1465.

11 V. Wang, N. Xu, J.-C. Liu, G. Tang and W.-T. Geng, *Comput. Phys. Commun.*, 2021, **267**, 108033.

12 E. Runge and E. K. U. Gross, *Phys. Rev. Lett.*, 1984, **52**, 997-1000.

13 M. J. Frisch, G. W. Trucks, H. B. Schlegel, G. E. Scuseria, M. A. Robb, J. R. Cheeseman, G. Scalmani, V. Barone, G. A. Petersson, H. Nakatsuji, X. Li, M. Caricato, A. V. Marenich, J. Bloino, B. G. Janesko, R. Gomperts, B. Mennucci, H. P. Hratchian, J. V. Ortiz, A. F. Izmaylov, J. L. Sonnenberg, Williams, F. Ding, F. Lipparini, F. Egidi, J. Goings, B. Peng, A. Petrone, T. Henderson, D. Ranasinghe, V. G. Zakrzewski, J. Gao, N. Rega, G. Zheng, W. Liang, M. Hada, M. Ehara, K. Toyota, R. Fukuda, J. Hasegawa, M. Ishida, T. Nakajima, Y. Honda, O. Kitao, H. Nakai, T. Vreven, K. Throssell, J. A. Montgomery Jr., J. E. Peralta, F. Ogliaro, M. J. Bearpark, J. J. Heyd, E. N. Brothers, K. N. Kudin, V. N. Staroverov, T. A. Keith, R. Kobayashi, J. Normand, K. Raghavachari, A. P. Rendell, J. C. Burant, S. S. Iyengar, J. Tomasi, M. Cossi, J. M. Millam, M. Klene, C. Adamo, R. Cammi, J. W. Ochterski, R. L. Martin, K. Morokuma, O. Farkas, J. B. Foresman, D. J. Fox, Wallingford, CT, 2016.

14 L. W. Chung, W. M. C. Sameera, R. Ramozzi, A. J. Page, M. Hatanaka, G. P. Petrova, T. V. Harris, X. Li, Z. Ke, F. Liu, H.-B. Li, L. Ding and K. Morokuma, *Chem. Rev.*, 2015, **115**, 5678-5796.

15 P. J. Hay and W. R. Wadt, *J. Chem. Phys.*, 1985, **82**, 299-310.

16 C. Adamo and V. Barone, *Chem. Phys. Lett.*, 1999, **314**, 152-157.

17 S. Grimme, J. Antony, S. Ehrlich and H. Krieg, *J. Chem. Phys.*, 2010, **132**, 154104.

18 Z. Shuai, *Chin. J. Chem.*, 2020, **38**, 1223-1232.